J. Fluid Mech. (2008), *vol.* 606, *pp.* 75–104.
doi:10.1017/S0022112008001572 Printed in the United Kingdom

On the motion of a porous sphere in a Stokes flow parallel to a planar confining boundary

B. C. ROY AND E. R. DAMIANO

Department of Biomedical Engineering, Boston University, Boston, MA 02215, USA

(Received 5 September 2007 and in revised form 15 March 2008)

An analysis is presented of the three-dimensional creeping flow in and around a porous sphere, modelled as a generalized Brinkman medium, near a smooth plane where the sphere (i) translates uniformly without rotating in an otherwise quiescent Newtonian fluid, (ii) rotates uniformly without translating in an otherwise quiescent Newtonian fluid, and (iii) is fixed in a shear field, which is uniform in the far field and has a linearly increasing velocity profile with increasing distance from the plane. The linear superposition of these three flow regimes is also considered for the special case of the free translational and rotational motion of a neutrally buoyant porous sphere in a shear field that is uniform in the far field. Exact series solutions to the momentum equations are derived for the velocity and pressure fields in the Brinkman and Stokes-flow regions. Coefficients in the series solutions for each flow regime are determined using recursion relations derived from the continuity equations in the Brinkman and Stokes-flow regions, from the interfacial boundary conditions on the porous spherical surface, and from the no-slip condition on the plane. Results are presented in terms of the drag force on the porous sphere and torque about the sphere centre as a function of the dimensionless clearance distance between the sphere and the rigid plane for several values of the dimensionless hydraulic permeability of the Brinkman medium. The free motion of the neutrally buoyant sphere is calculated by requiring that the net hydrodynamic drag force and torque acting on the sphere vanish. Results for this case are presented in terms of the dimensionless translational and rotational speeds of the porous sphere relative to the far-field shear rate as a function of the dimensionless clearance distance for several values of the dimensionless hydraulic permeability. The work is motivated by insights it offers into the behaviour of porous agglomerates, and by its potential utility in industrial, biological, biophysical, medicinal and environmental applications wherever gas or liquid suspensions of porous agglomerates might arise.

1. Introduction

The hydrodynamic interactions that arise between rigid solids of revolution in a Stokes flow near solid boundaries, between rigid solids of revolution in a Stokes flow near porous media, and in creeping flows inside and around porous bodies in an unbounded medium, have been the subject of numerous studies over the years (Weinbaum, Ganatos & Yan 1990). The early studies by Jeffery and coworkers (Jeffrey 1915; Stimson & Jeffery 1926) and later by O'Neill and coworkers (Dean & O'Neill 1963; O'Neill 1964; Goren & O'Neill 1971) used bispherical coordinates to obtain exact series solutions for Stokes flows induced by the motion or presence of a solid sphere near planar confining boundaries or other spherical bodies. The work of

O'Neill and coworkers led to exact series solutions of the fully three-dimensional Stokes equations for flow induced by a solid sphere near a smooth plane where the sphere is (i) under pure rotation without translation in an otherwise quiescent fluid (Dean & O'Neill 1963), (ii) in uniform translation without rotation in an otherwise quiescent fluid (O'Neill 1964), and (iii) stationary in a shear field, which is uniform in the far field and has a linearly increasing velocity profile with increasing distance from the plane (Goren & O'Neill 1971). Since the governing differential equations and boundary conditions of these three elemental problems are linear, their solutions can be linearly superposed to provide the solution to the more complicated Stokes flow arising from the free translational and rotational motion of a neutrally buoyant solid sphere near a plane wall where the shear field is uniform in the far field. For this problem, Goldman, Cox & Brenner (1967) imposed the condition that the net hydrodynamic force and torque about the centre of a neutrally buoyant solid sphere must vanish, and obtained asymptotic expressions for the translational and rotational speeds of the sphere as a function of the dimensionless clearance distance between the sphere and the plane.

All three elemental problems (translation, rotation, and uniform shear), as well as the linear superposition of these solutions for the neutrally buoyant case, were generalized by Damiano *et al.* (2004*a*) to the fully three-dimensional problem of the Stokes flow around a solid sphere near a porous planar medium. The porous medium was modelled as a Brinkman half-space, where asymptotic approximations of the exact integral solutions were found for the flow in the Brinkman medium, and the exact infinite series solutions, first obtained by Dean & O'Neill (1963), were used for the Stokes flow around the sphere. Whereas the degenerate problem of a planar confining boundary was characterized by a single parameter (the dimensionless clearance between the solid sphere and the plane), the generalized problem of the planar porous medium spans a two-dimensional parameter space, which consists of the dimensionless clearance between the solid sphere and the porous interface, and the dimensionless Brinkman parameter, $a\,(K/\mu)^{1/2}$ (where a is the sphere radius and μ/K is the Darcy permeability of the Brinkman medium), which characterizes the ratio of permeation-induced viscous drag forces associated with fluid motion through the pores of the Brinkman medium to viscous drag forces associated with fluid-velocity gradients within the Brinkman medium.

Brinkman (1947) proposed an equation to model flow through porous media that contains a Newtonian viscous drag term and a Darcy drag term which together balance the pressure gradient. The so-called 'Brinkman equation' can be regarded as a particular limit of the more general equations of binary mixture theory, which derive from the continuum field theory of heterogeneous materials (Truesdell & Toupin 1960). In particular, when inertial forces are negligible, i.e. in the limit of vanishing Reynolds number, and in the limit as the solid-volume fraction, ϕ^s, of the mixture vanishes, the equation governing the fluid constituent in the mixture corresponds to the Brinkman equation provided that the Brinkman medium itself is in an inertial frame and the reference coordinates are affixed to that frame. In binary mixture theory, the conservation equations for the fluid constituent of the porous medium and the conditions on the velocity and stress fields at interfaces between the porous medium and fluid and solid boundaries are similar in form to those that arise for a Brinkman medium (Truesdell & Toupin 1960; Saffman 1971; Hou *et al.* 1989); however additional parameters are needed to characterize such a material and the deformation of the solid constituent of the mixture becomes a dependent field variable which is coupled to the motion of the fluid constituent.

In the present study, we consider the complementary problem to that considered by Damiano *et al.* (2004*a*). Namely, we will detail the three-dimensional flow that arises in and around a porous sphere, modelled as a generalized Brinkman medium, that is maintained at a constant distance from a smooth plane and is (i) under pure rotation without translation in an otherwise quiescent Newtonian fluid, (ii) in uniform translation without rotation in an otherwise quiescent Newtonian fluid, and (iii) stationary in a shear field, which is uniform in the far field and has a linearly increasing velocity profile with increasing distance from the plane. By virtue of the linearity of these boundary-value problems, we also consider the linear superposition of these three elemental problems to solve for the free translational and rotational motion of a neutrally buoyant porous sphere near a plane wall where the shear field is uniform in the far field. The significant solutions thus obtained consist of series solutions in terms of Legendre polynomials, which exactly satisfy the governing momentum equations for the velocity field and Laplace's equation for the pressure, in the Stokes-flow region above the plane and around the porous sphere, and throughout the Brinkman region within the porous sphere. For each of the flow regimes considered, the no-slip boundary condition is applied on the rigid plane, and continuity of the velocity and stress-traction vectors is imposed across the interfacial spherical surface separating the Stokes-flow region outside the porous sphere from the Brinkman region inside the porous sphere. Twelve recursion relations are derived to determine the coefficients in the series solutions such that those solutions exactly satisfy the boundary and interfacial conditions as well as the continuity equations in both the Stokes-flow and Brinkman regions.

This analysis complements not only the work of Damiano *et al.* (2004*a*), but also the work of Davis (2001), which considered the two-dimensional axisymmetric flow induced by the motion of a porous sphere translating perpendicular to a rigid plane, and the work of Feng, Ganatos & Weinbaum (1998), which considered the motion of a solid sphere through a Brinkman medium near planar confining boundaries. Motivation for this work lies in understanding the behaviour of porous agglomerates, which occur as gas or liquid suspensions in industrial, biological, biophysical, medicinal and environmental applications. Agglomerates can be viewed as continuum bodies, permeable to the surrounding medium, which could be gas or liquid (Vainshtein, Shapiro & Gutfinger 2004). The hydrodynamic interactions detailed here, between a porous sphere and a planar confining boundary, help extend our understanding of important processes such as coagulation rate (Saffman & Turner 1956), particle settling (Kim & Stolzenbach 2004), and the effective viscosity of porous agglomerates in solution (Vainshtein & Shapiro 2006) near planar substrates.

2. General formulation

Consider the Stokes flow, parallel to a planar confining boundary, P, of a fluid having constant viscosity, μ, that is induced or altered by the motion or presence of a porous sphere, itself modelled as a generalized Brinkman medium occupying the spherical volume, S, bounded by the closed surface, ∂S, and having constant viscosity, μ, and constant hydraulic resistivity, K (see figure 1). The mass and momentum conservation equations for the solenoidal flow fields throughout the Stokes-flow and spherical Brinkman regions are given respectively by

$$-\mu\nabla\times\nabla\times\tilde{\boldsymbol{v}}^{*}=\nabla\tilde{p}^{*},\quad \nabla\cdot\tilde{\boldsymbol{v}}^{*}=0,\quad \forall\ \boldsymbol{x}^{*}\notin S, \tag{2.1}$$

$$-\mu\nabla\times\nabla\times\boldsymbol{v}^{*}-K\left(\boldsymbol{v}^{*}-\boldsymbol{v}^{*s}\right)=\nabla p^{*},\quad \nabla\cdot\boldsymbol{v}^{*}=0,\quad \forall\ \boldsymbol{x}^{*}\in S, \tag{2.2}$$

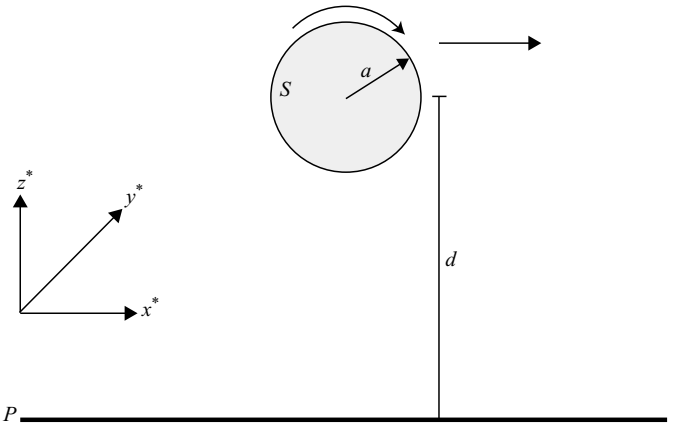

FIGURE 1. Schematic depicting the translational and rotational motion of a porous sphere, occupying a region S bounded by ∂S, in a Stokes flow bounded by a planar confining boundary, P.

where $\tilde{\boldsymbol{v}}^*$ is the dimensional fluid velocity vector in the Stokes-flow region, $\boldsymbol{v}^*$ is the dimensional fluid velocity vector in the spherical Brinkman region, bounded by ∂S, $\boldsymbol{v}^{*s}$ is the dimensional velocity associated with the local rigid-body motion of 'solid constituent' of the porous sphere, and $\tilde{p}^*$ and p^* denote the dimensional pressure fields in the Stokes-flow and Brinkman regions, respectively (variables that carry a tilde are associated with the Stokes-flow region, variables that carry an asterisk are dimensional). Taking the divergence of the momentum equations and using the fact that both velocity fields are solenoidal, it follows that $\boldsymbol{\nabla}\cdot\boldsymbol{\nabla}\tilde{p}^* = \nabla^2\tilde{p}^* = 0$ and $\boldsymbol{\nabla}\cdot\boldsymbol{\nabla}p^* = \nabla^2 p^* = 0$ throughout their respective fields.

More precisely, (2.2) corresponds to the momentum equation of the fluid constituent associated with a binary mixture in the limit of vanishing Reynolds number and vanishing solid-volume fraction, ϕ^s, where it is understood that the solid constituent is non-deformable and undergoes rigid-body motion only. Owing to this rigid-body motion, which is embodied in $\boldsymbol{v}^{*s}$, we regard (2.2) as a generalized form of the Brinkman equation.

3. Brinkman equations in cylindrical coordinates

Consider the Cartesian coordinate system, (x^*, y^*, z^*), as shown in figure 1. Let the rigid planar confining boundary, P, herein referred to as the reference plane, be located at $z^* = 0$. The dimensional fluid velocity vector in the spherical Brinkman region is given in Cartesian coordinates (x^*, y^*, z^*) by $\boldsymbol{v}^* = v_x^*\boldsymbol{e}_x + v_y^*\boldsymbol{e}_y + v_z^*\boldsymbol{e}_z$, where $\boldsymbol{x}^* = x^*\boldsymbol{e}_x + y^*\boldsymbol{e}_y + z^*\boldsymbol{e}_z$. In cylindrical coordinates (r^*, θ, z^*), where $x^* = r^*\cos\theta$, $y^* = r^*\sin\theta$, and $\boldsymbol{v}^* = v_r^*\boldsymbol{e}_r + v_\theta^*\boldsymbol{e}_\theta + v_z^*\boldsymbol{e}_z$, the governing conservation equations in the spherical Brinkman region, given by (2.2), take the form

$$\nabla^2 v_r^* - \frac{v_r^*}{r^{*2}} - \frac{2}{r^{*2}}\frac{\partial v_\theta^*}{\partial\theta} - \frac{K}{\mu}\left(v_r^* - v_r^{*s}\right) = \frac{1}{\mu}\frac{\partial p^*}{\partial r^*}, \tag{3.1}$$

$$\nabla^2 v_\theta^* - \frac{v_\theta^*}{r^{*2}} + \frac{2}{r^{*2}}\frac{\partial v_r^*}{\partial\theta} - \frac{K}{\mu}\left(v_\theta^* - v_\theta^{*s}\right) = \frac{1}{\mu\, r^*}\frac{\partial p^*}{\partial\theta}, \tag{3.2}$$

$$\nabla^2 v_z^* - \frac{K}{\mu}\left(v_z^* - v_z^{*s}\right) = \frac{1}{\mu}\frac{\partial p^*}{\partial z^*}, \tag{3.3}$$

$$\frac{\partial v_r^*}{\partial r^*} + \frac{v_r^*}{r^*} + \frac{1}{r^*}\frac{\partial v_\theta^*}{\partial \theta} + \frac{\partial v_z^*}{\partial z^*} = 0, \tag{3.4}$$

where the scalar Laplacian is defined as

$$\nabla^2 = \frac{\partial^2}{\partial r^{*2}} + \frac{1}{r^*}\frac{\partial}{\partial r^*} + \frac{1}{r^{*2}}\frac{\partial^2}{\partial \theta^2} + \frac{\partial^2}{\partial z^{*2}}.$$

The velocity vector, $\boldsymbol{v}^{*s} = v_r^{*s}\boldsymbol{e}_r + v_\theta^{*s}\boldsymbol{e}_\theta + v_z^{*s}\boldsymbol{e}_z$, for the three different flow regimes associated with the sphere motions considered here is defined as follows:

(*a*) when the sphere is stationary near P in a flow that approaches a uniform shear field, of strength $\dot{\gamma}$, in the far field, $\boldsymbol{v}^{*s}$ is given in Cartesian coordinates by

$$\boldsymbol{v}^{*s}(\boldsymbol{x}^*) = \boldsymbol{0}, \quad \forall\ \boldsymbol{x}^* \in S$$

and in cylindrical coordinates by

$$\boldsymbol{v}^{*s}(r^*, \theta, z^*) = \boldsymbol{0}, \quad \forall\ (r^*, \theta, z^*) \in S; \tag{3.5}$$

(*b*) when the sphere undergoes a purely steady translational motion, parallel to P with constant speed U in the positive x^*-direction through an otherwise quiescent fluid, $\boldsymbol{v}^{*s}$ is given in Cartesian coordinates by

$$\boldsymbol{v}^{*s}(\boldsymbol{x}^*) = U\boldsymbol{e}_x, \quad \forall\ \boldsymbol{x}^* \in S$$

and in cylindrical coordinates by

$$\boldsymbol{v}^{*s}(r^*, \theta, z^*) = U\,(\cos\theta\,\boldsymbol{e}_r - \sin\theta\,\boldsymbol{e}_\theta), \quad \forall\ (r^*, \theta, z^*) \in S; \tag{3.6}$$

(*c*) when the sphere undergoes a purely steady rotational motion about an axis parallel to P with constant speed Ω in the positive y^*-direction through an otherwise quiescent fluid, $\boldsymbol{v}^{*s}$ is given by

$$\boldsymbol{v}^{*s}(\boldsymbol{x}^*) = \Omega\,\boldsymbol{e}_y \times \boldsymbol{r}^{*s}, \quad \forall\ \boldsymbol{x}^* \in S,$$

where $\boldsymbol{r}^{*s}$ is the position vector originating from the sphere centre to any point in S. In Cartesian coordinates, this takes the form

$$\boldsymbol{v}^{*s} = \Omega\left((z^* - d)\,\boldsymbol{e}_x - x^*\,\boldsymbol{e}_z\right), \quad \forall\ (x^*, y^*, z^*) \in S,$$

where d is the distance from the plane to the centre of the sphere located at $\boldsymbol{x}^* = d\,\boldsymbol{e}_z$. In cylindrical coordinates this takes the form

$$\boldsymbol{v}^{*s}(r^*, \theta, z^*) = \Omega\left((z^* - d)(\cos\theta\,\boldsymbol{e}_r - \sin\theta\,\boldsymbol{e}_\theta) - r^*\cos\theta\,\boldsymbol{e}_z\right), \quad \forall\ (r^*, \theta, z^*) \in S. \tag{3.7}$$

These three flow regimes are collectively represented by the single expression for $\boldsymbol{v}^{*s}$ given by

$$\boldsymbol{v}^{*s}(r^*, \theta, z^*) = V((c_t + c_r(z^* - d))\cos\theta\boldsymbol{e}_r - (c_t + c_r(z^* - d))\sin\theta\boldsymbol{e}_\theta - c_r r^*\cos\theta\boldsymbol{e}_z), \tag{3.8}$$

where, for purely translational motion of the sphere in an otherwise quiescent fluid, $c_t = 1$, $c_r = 0$ and $V = U$, for purely rotational motion of the sphere in an otherwise quiescent fluid, $c_t = 0$, $c_r = 1$ and $V = c\,\Omega$, and for a stationary sphere where the flow approaches a uniform shear field, of strength $\dot{\gamma}$, in the far field, $c_t = c_r = 0$ and $V = c\,\dot{\gamma}$, where c is a characteristic length scale defined below.

Following the approach of Dean & O'Neill (1963), the θ-dependence of equations (3.1)–(3.4) can be eliminated from the problem and useful decoupling occurs if p^* and the cylindrical components of $\boldsymbol{v}^*$ are written as

$$p^* = \frac{\mu V}{c}Q(r, z)\cos\theta, \quad v_r^* = \tfrac{1}{2}V\,(r\,Q(r, z) + U_0(r, z) + U_2(r, z))\cos\theta, \tag{3.9}$$

$$v_\theta^* = \tfrac{1}{2}V\,(U_2(r,z) - U_0(r,z))\sin\theta, \quad v_z^* = \tfrac{1}{2}V\,(zQ(r,z) + 2w(r,z))\cos\theta, \quad (3.10)$$

where V is the characteristic velocity defined for each of the three flow regimes described above, $\boldsymbol{v} = \boldsymbol{v}^*/V$, $p = cp^*/(\mu V)$, $r = r^*/c$, and $z = z^*/c$. For a sphere of radius a in the Stokes-flow region, the characteristic length scale $c = (d^2 - a^2)^{1/2}$. It is convenient to choose c as our characteristic length scale since this will render the transformation we introduce below, between dimensionless cylindrical coordinates and spherical coordinates, free of parameters. This, in turn, will simplify the form of many of the expressions that we will derive that will use the spherical coordinate system.

When (3.8) and the decoupling relations, given by (3.9) and (3.10), are substituted into the conservation equations, the fully three-dimensional problem reduces to one that is dependent only on r and z. In particular, (3.1)–(3.4) and Laplace's equation for the pressure, p^*, are satisfied throughout the spherical Brinkman region if

$$\mathrm{L}_1^2\,Q = 0, \qquad \mathrm{L}_1^2\,w - \epsilon^{-2}\left(w + \tfrac{1}{2}zQ + c_r r\right) = 0, \quad (3.11)$$

$$\mathrm{L}_0^2\,U_0 - \epsilon^{-2}\left(U_0 + \tfrac{1}{2}rQ - 2c_t - 2c_r\,(z - d/c)\right) = 0, \qquad \mathrm{L}_2^2\,U_2 - \epsilon^{-2}\left(U_2 + \tfrac{1}{2}rQ\right) = 0, \quad (3.12)$$

$$\left(3 + r\frac{\partial}{\partial r} + z\frac{\partial}{\partial z}\right)Q + \frac{\partial U_0}{\partial r} + \left(\frac{\partial}{\partial r} + \frac{2}{r}\right)U_2 + 2\frac{\partial w}{\partial z} = 0, \quad (3.13)$$

where

$$\mathrm{L}_m^2 = \frac{\partial^2}{\partial r^2} + \frac{1}{r}\frac{\partial}{\partial r} - \frac{m^2}{r^2} + \frac{\partial^2}{\partial z^2}.$$

In (3.11) and (3.12), the dimensionless hydraulic permeability of the Brinkman medium, $\epsilon^2 = \mu/(Kc^2)$, characterizes the ratio of viscous drag forces associated with fluid-velocity gradients in the spherical Brinkman region to permeation-induced viscous drag forces associated with fluid motion relative to the 'solid constituent' of the porous sphere.

4. Cylindrical components of the Brinkman equations in spherical coordinates

Since the Brinkman medium has a spherical geometry, it is convenient to express the cylindrical components of the velocity field in S in terms of the spherical coordinates (ϱ, θ, ϕ), which are related to the cylindrical coordinates (r, θ, z) according to

$$r = \varrho\sin\phi, \quad z = \varrho\cos\phi + d/c \quad (0 \leqslant \varrho \leqslant a/c, 0 \leqslant \phi \leqslant \pi), \quad (4.1)$$

where the origin of the spherical coordinate system is located at the centre of the sphere, i.e. at $z = d/c$.

Using the chain rule of differentiation to express r- and z-derivatives and the differential operator L_m^2 in terms of the spherical coordinates, ϱ and ϕ, the conservation equations governing the flow field throughout the spherical Brinkman region, given by (3.11)–(3.13), are satisfied if

$$\mathsf{L}_1^2\,Q = 0, \quad \mathsf{L}_1^2\,w = \frac{1}{\epsilon^2}\Big(w + \tfrac{1}{2}\,(\varrho\cos\phi + d/c)\;Q + c_r\varrho\sin\phi\Big), \quad (4.2)$$

$$\mathsf{L}_0^2\,U_0 = \frac{1}{\epsilon^2}\Big(U_0 + \tfrac{1}{2}\varrho\sin\phi\;Q - 2\,(c_t + c_r\varrho\cos\phi)\Big), \quad \mathsf{L}_2^2\,U_2 = \frac{1}{\epsilon^2}\Big(U_2 + \tfrac{1}{2}\varrho\sin\phi\;Q\Big), \quad (4.3)$$

$$\left(3+\varrho\frac{\partial}{\partial\varrho}\right)Q+\frac{2\,U_2}{\varrho\sin\phi}+\left(\sin\phi\frac{\partial}{\partial\varrho}+\frac{\cos\phi}{\varrho}\frac{\partial}{\partial\phi}\right)(U_0+U_2)$$
$$+\left(\cos\phi\frac{\partial}{\partial\varrho}-\frac{\sin\phi}{\varrho}\frac{\partial}{\partial\phi}\right)\left(\frac{d}{c}Q+2w\right)=0, \quad (4.4)$$

where

$$\mathsf{L}_m^2=\frac{\partial^2}{\partial\varrho^2}+\frac{2}{\varrho}\frac{\partial}{\partial\varrho}+\frac{\cot\phi}{\varrho^2}\frac{\partial}{\partial\phi}+\frac{1}{\varrho^2}\frac{\partial^2}{\partial\phi^2}-\frac{m^2}{\varrho^2\sin^2\phi}. \quad (4.5)$$

5. Cylindrical components of the Stokes equations in bispherical coordinates

The cylindrical-coordinate representation of the equations associated with the Stokes-flow region are given by (3.1)–(3.4) and (3.11)–(3.13), when K and ϵ^{-2} vanish, and tildes are added to all dependent variables. However, owing to the presence of the sphere in the Stokes-flow region, cylindrical coordinates are not an ideal choice. On the other hand, since the reference plane, P, is a degenerate sphere in the limit of infinite radius of curvature, it is convenient to express the cylindrical components of the velocity field in the Stokes-flow region in terms of bispherical coordinates (η,θ,ξ), which are related to the cylindrical coordinates (r,θ,z) according to

$$r=\frac{\sin\eta}{\cosh\xi-\cos\eta}, \quad z=\frac{\sinh\xi}{\cosh\xi-\cos\eta} \quad (0\leqslant\eta\leqslant\pi,\,0\leqslant\xi\leqslant\alpha). \quad (5.1)$$

The coordinate surface $\xi=\alpha>0$ corresponds to the locus of points that lie on the spherical interfacial surface, ∂S, which is the only coordinate surface that the spherical and bispherical coordinate systems share, while the coordinate surface $\xi=z=0$ corresponds to the locus of points that lie on the reference plane, P, which is the only coordinate surface that the cylindrical and bispherical coordinate systems share. Using the chain rule of differentiation to express r- and z-derivatives and the differential operator L_m^2 in terms of the bispherical coordinates, η and ξ, the conservations equations governing the flow field throughout the Stokes-flow region, given by (3.11)–(3.13), with tildes added to all dependent variables and $\epsilon^{-2}=0$, are satisfied if

$$\mathscr{L}_1^2\,\tilde{Q}=\mathscr{L}_1^2\,\tilde{w}=\mathscr{L}_0^2\,\tilde{U}_0=\mathscr{L}_2^2\,\tilde{U}_2=0, \quad (5.2)$$

$$3\,\tilde{Q}+2\,\mathrm{cosec}\,\eta\,(\cosh\xi-\cos\eta)\,\tilde{U}_2-\cos\eta\sinh\xi\,\frac{\partial\tilde{Q}}{\partial\xi}-\sin\eta\cosh\xi\,\frac{\partial\tilde{Q}}{\partial\eta}$$
$$-(1-\cos\eta\cosh\xi)\left(\frac{\partial\tilde{U}_0}{\partial\eta}+\frac{\partial\tilde{U}_2}{\partial\eta}-2\frac{\partial\tilde{w}}{\partial\xi}\right)-\sin\eta\sinh\xi\left(\frac{\partial\tilde{U}_0}{\partial\xi}+\frac{\partial\tilde{U}_2}{\partial\xi}+2\frac{\partial\tilde{w}}{\partial\eta}\right)=0, \quad (5.3)$$

where

$$\mathscr{L}_m^2=\frac{\partial^2}{\partial\eta^2}+\frac{\partial^2}{\partial\xi^2}+\frac{1-\cos\eta\cosh\xi}{\sin\eta\,(\cos\eta-\cosh\xi)}\frac{\partial}{\partial\eta}+\frac{\sinh\xi}{\cos\eta-\cosh\xi}\frac{\partial}{\partial\xi}-\frac{m^2}{\sin^2\eta}. \quad (5.4)$$

We can generalize, slightly, the decoupling relations introduced in (3.9) and (3.10) in order to collectively account for all three flow regimes to be considered here. In particular, the Stokes-flow equations decouple if $\tilde{p}^*$ and the cylindrical components

of $\tilde{\boldsymbol{v}}^*$ are written as

$$\tilde{p}^* = \frac{\mu V}{c}\tilde{Q}(r,z)\cos\theta, \quad \tilde{v}_r^* = \tfrac{1}{2}V\left(r\tilde{Q}(r,z) + \tilde{U}_0(r,z) + \tilde{U}_2(r,z) + c_s z\right)\cos\theta, \quad (5.5)$$

$$\tilde{v}_\theta^* = \tfrac{1}{2}V\left(\tilde{U}_2(r,z) - \tilde{U}_0(r,z) - c_s z\right)\sin\theta, \quad \tilde{v}_z^* = \tfrac{1}{2}V\left(z\tilde{Q}(r,z) + 2\tilde{w}(r,z)\right)\cos\theta, \quad (5.6)$$

where $\tilde{\boldsymbol{v}}^*$ and $\tilde{p}^*$ are non-dimensionalized in the same manner as $\boldsymbol{v}^*$ and p^*.

If the Stokes flow is induced by the either translational or rotational motion of the porous sphere, then $V = U$ or $V = c\,\Omega$, respectively, and $c_s = 0$. However, for a stationary sphere in a flow that approaches a uniform shear field in the far field, $V = c\,\dot{\gamma}$, and $c_s = 2$. Since adding to $\tilde{v}_r^*$ and subtracting from $\tilde{v}_\theta^*$ the same linear function of z does not change the left-hand sides of (3.1) and (3.2) when $K = 0$, the differential equations governing $\tilde{Q}$, $\tilde{w}$, $\tilde{U}_0$ and $\tilde{U}_2$, are identical for all three flow regimes considered here and are still given by (5.2)–(5.4).

6. Exact solution of the governing equations

Below we provide general forms of the exact solutions to (4.2), (4.3) and (5.2) and the conditions under which those solutions can be made to satisfy the continuity equations given by (4.4) and (5.3).

6.1. *Solution in the spherical Brinkman region*

On solving equations (4.2) and (4.3) by the method of separation of variables, we find that, to within the arbitrary constants a_n, c_n, e_n and g_n, the exact solution for flow in the spherical Brinkman region is given by

$$Q(\varrho,\phi) = \sum_{n=1}^{\infty} c_n\,\varrho^n \sin\phi\; P_n'(\cos\phi), \quad (6.1)$$

$$w(\varrho,\phi) = -c_r\,\varrho\,\sin\phi - \tfrac{1}{2}(\varrho\cos\phi + d/c)\,Q - \epsilon^2\left(\cos\phi\frac{\partial Q}{\partial\varrho} - \frac{\sin\phi}{\varrho}\frac{\partial Q}{\partial\phi}\right) + \sum_{n=1}^{\infty} a_n \frac{I_{n+1/2}(\varrho/\epsilon)}{\varrho^{1/2}}\sin\phi\; P_n'(\cos\phi), \quad (6.2)$$

$$U_0(\varrho,\phi) = 2\,c_t + 2\,c_r\,\varrho\cos\phi - \tfrac{1}{2}\varrho\sin\phi\;Q - \epsilon^2\left(\frac{Q}{\varrho\sin\phi} + \sin\phi\frac{\partial Q}{\partial\varrho} + \frac{\cos\phi}{\varrho}\frac{\partial Q}{\partial\phi}\right) + \sum_{n=0}^{\infty} e_n \frac{I_{n+1/2}(\varrho/\epsilon)}{\varrho^{1/2}}P_n(\cos\phi), \quad (6.3)$$

$$U_2(\varrho,\phi) = -\tfrac{1}{2}\varrho\sin\phi\;Q + \epsilon^2\left(\frac{Q}{\varrho\sin\phi} - \sin\phi\frac{\partial Q}{\partial\varrho} - \frac{\cos\phi}{\varrho}\frac{\partial Q}{\partial\phi}\right) + \sum_{n=2}^{\infty} g_n \frac{I_{n+1/2}(\varrho/\epsilon)}{\varrho^{1/2}}\sin^2\phi\; P_n''(\cos\phi), \quad (6.4)$$

where $I_{n+1/2}$ is the modified Bessel function of the first kind, P_n are the Legendre polynomials of the first kind, and the primes denote differentiation with respect to $\cos\phi$. Note that $\varrho^{-(n+1)}$, corresponding to the second linearly independent complementary solution associated with Q, and $K_{n+1/2}(\varrho/\epsilon)/\varrho^{1/2}$, corresponding to

the second linearly independent complementary solution associated with w, U_0 and U_2, grow without bound in the spherical Brinkman region as $\varrho \to 0$, and are therefore not admissible. On the other hand, it can be shown using L'Hopital's rule that $I_{n+1/2}(\varrho/\epsilon)/\varrho^{1/2}$, the admissible complementary solution associated with w, U_0 and U_2, is bounded in the spherical Brinkman region as $\varrho \to 0$.

Substituting (6.1)–(6.4) into the continuity equation, given by (4.4), and using the recursion relations for the Legendre polynomials, one obtains a solenoidal velocity field throughout the spherical Brinkman region if

$$(2n+3)(e_{n-1}+2(n-1)a_{n-1}-(n-1)(n-2)g_{n-1}) - (2n-1)(e_{n+1}+2(n+2)a_{n+1}-(n+2)(n+3)g_{n+1})=0, \quad n=1,2,\ldots. \tag{6.5}$$

Note that this recursion relation satisfies the continuity equation in the spherical Brinkman region irrespective of the motion of the sphere being translational, rotational, or stationary.

6.2. *Solution in the Stokes-flow region*

Following Dean & O'Neill (1963), the series solutions that exactly satisfy (5.2) are given by

$$\tilde{Q}(\eta,\xi)=\sin\eta\,(\cosh\xi-\cos\eta)^{1/2}\sum_{n=1}^{\infty}\left(\tilde{c}_n\cosh\left(n+\tfrac{1}{2}\right)\xi+\tilde{d}_n\sinh\left(n+\tfrac{1}{2}\right)\xi\right)P_n'(\cos\eta), \tag{6.6}$$

$$\tilde{w}(\eta,\xi)=\sin\eta\,(\cosh\xi-\cos\eta)^{1/2}\sum_{n=1}^{\infty}\left(\tilde{a}_n\cosh\left(n+\tfrac{1}{2}\right)\xi+\tilde{b}_n\sinh\left(n+\tfrac{1}{2}\right)\xi\right)P_n'(\cos\eta), \tag{6.7}$$

$$\tilde{U}_0(\eta,\xi)=(\cosh\xi-\cos\eta)^{1/2}\sum_{n=0}^{\infty}\left(\tilde{e}_n\cosh\left(n+\tfrac{1}{2}\right)\xi+\tilde{f}_n\sinh\left(n+\tfrac{1}{2}\right)\xi\right)P_n(\cos\eta), \tag{6.8}$$

$$\tilde{U}_2(\eta,\xi)=\sin^2\eta\,(\cosh\xi-\cos\eta)^{1/2}\sum_{n=2}^{\infty}\left(\tilde{g}_n\cosh\left(n+\tfrac{1}{2}\right)\xi+\tilde{h}_n\sinh\left(n+\tfrac{1}{2}\right)\xi\right)P_n''(\cos\eta), \tag{6.9}$$

where the primes denote differentiation with respect to $\cos\eta$.

Substituting (6.6)–(6.9) into the continuity equation, given by (5.3), and using the recursion relations for the Legendre polynomials, one obtains a solenoidal velocity field throughout the Stokes-flow region if

$$\tfrac{5}{2}\tilde{d}_n-\tfrac{1}{2}((n-1)\tilde{d}_{n-1}-(n+2)\tilde{d}_{n+1})-\tfrac{1}{2}(\tilde{f}_{n-1}-2\tilde{f}_n+\tilde{f}_{n+1}) +\tfrac{1}{2}((n-2)(n-1)\tilde{h}_{n-1}-2(n-1)(n+2)\tilde{h}_n+(n+2)(n+3)\tilde{h}_{n+1}) -(n-1)\tilde{a}_{n-1}+(2n+1)\tilde{a}_n-(n+2)\tilde{a}_{n+1}=0, \quad n=1,2,\ldots \tag{6.10}$$

and

$$\tfrac{5}{2}\tilde{c}_n-\tfrac{1}{2}((n-1)\tilde{c}_{n-1}-(n+2)\tilde{c}_{n+1})-\tfrac{1}{2}(\tilde{e}_{n-1}-2\tilde{e}_n+\tilde{e}_{n+1}) +\tfrac{1}{2}((n-2)(n-1)\tilde{g}_{n-1}-2(n-1)(n+2)\tilde{g}_n+(n+2)(n+3)\tilde{g}_{n+1}) -(n-1)\tilde{b}_{n-1}+(2n+1)\tilde{b}_n-(n+2)\tilde{b}_{n+1}=0, \quad n=1,2,\ldots. \tag{6.11}$$

7. Boundary conditions on the reference plane

The Stokes-flow region is bounded by the reference plane, P, where the no-slip boundary condition requires that $\tilde{\boldsymbol{v}}(\boldsymbol{x}) = \boldsymbol{0}, \forall\ \boldsymbol{x} \in P$. In cylindrical coordinates, this boundary condition takes the form

$$\tilde{v}_r = \tilde{v}_\theta = \tilde{v}_z = 0, \quad \forall\ (r, \theta) \in z = 0. \tag{7.1}$$

Using the decoupling relations, given by (5.5) and (5.6), the no-slip boundary condition is satisfied if

$$\tilde{w}(r, 0) = \tilde{U}_0(r, 0) + \tfrac{1}{2} r \tilde{Q}(r, 0) = \tilde{U}_2(r, 0) + \tfrac{1}{2} r \tilde{Q}(r, 0) = 0. \tag{7.2}$$

In bispherical coordinates (η, ξ), where the reference plane, P, corresponds to the coordinate surface $\xi = 0$, these conditions are given by

$$\tilde{w}(\eta, 0) = \tilde{U}_0(\eta, 0) + \tfrac{1}{2} \frac{\sin\eta}{1 - \cos\eta} \tilde{Q}(\eta, 0) = \tilde{U}_2(\eta, 0) + \tfrac{1}{2} \frac{\sin\eta}{1 - \cos\eta} \tilde{Q}(\eta, 0) = 0. \tag{7.3}$$

Substituting the series solutions, given by (6.6)–(6.9), into (7.3), and making use of the recursion relations for the Legendre polynomials, the no-slip boundary condition on the reference plane, P, is satisfied if

$$\frac{(n+1)(n+2)}{2(2n+3)} \tilde{c}_{n+1} - \frac{n(n-1)}{2(2n-1)} \tilde{c}_{n-1} - \frac{n}{2n-1} \tilde{e}_{n-1} + \tilde{e}_n - \frac{n+1}{2n+3} \tilde{e}_{n+1} = 0, \quad n = 0, 1, \ldots, \tag{7.4}$$

$$\tilde{a}_n = 0, \quad n = 1, 2, \ldots, \tag{7.5}$$

$$\frac{1}{2(2n-1)} \tilde{c}_{n-1} - \frac{1}{2(2n+3)} \tilde{c}_{n+1} - \frac{n-2}{2n-1} \tilde{g}_{n-1} + \tilde{g}_n - \frac{n+3}{2n+3} \tilde{g}_{n+1} = 0, \quad n = 2, 3, \ldots. \tag{7.6}$$

In the light of (7.5), the first recursion relation derived from the continuity equation, given by (6.10), thus reduces to

$$\begin{aligned} &\tfrac{5}{2} \tilde{d}_n - \tfrac{1}{2}((n-1)\tilde{d}_{n-1} - (n+2)\tilde{d}_{n+1}) - \tfrac{1}{2}(\tilde{f}_{n-1} - 2\tilde{f}_n + \tilde{f}_{n+1}) \\ &\quad + \tfrac{1}{2}((n-2)(n-1)\tilde{h}_{n-1} - 2(n-1)(n+2)\tilde{h}_n + (n+2)(n+3)\tilde{h}_{n+1}) = 0, \\ &\qquad\qquad n = 1, 2, \ldots. \end{aligned} \tag{7.7}$$

8. Interfacial velocity and stress conditions

We require that the velocity vector and Cauchy stress tensor be continuous across the interfacial surface, ∂S, separating the spherical Brinkman region and the Stokes-flow region. In particular, if $\boldsymbol{n}$ is an outwardly facing unit vector that is locally orthogonal to the spherical interface, ∂S, then the stress traction vector acting on ∂S is given by $\boldsymbol{\sigma}^* \cdot \boldsymbol{n}$, where $\boldsymbol{\sigma}^*$ is the dimensional Cauchy stress tensor. The interfacial velocity and stress conditions are then given by

$$\boldsymbol{v}^*(\boldsymbol{x}^*) = \tilde{\boldsymbol{v}}^*(\boldsymbol{x}^*), \quad \boldsymbol{\sigma}^*(\boldsymbol{x}^*) \cdot \boldsymbol{n} = -\tilde{\boldsymbol{\sigma}}^*(\boldsymbol{x}^*) \cdot \tilde{\boldsymbol{n}}, \quad \forall\ \boldsymbol{x}^* \in \partial S, \tag{8.1a,b}$$

where $\boldsymbol{n} = \boldsymbol{e}_\varrho = \sin\phi\, \boldsymbol{e}_r + \cos\phi\, \boldsymbol{e}_z$ and $\tilde{\boldsymbol{n}} = -\boldsymbol{e}_\varrho$ are, respectively, the outwardly facing unit normal vectors to the spherical Brinkman and Stokes-flow regions on ∂S. Equation (8.1b) asserts that the stress-traction vectors associated with the Stokes-flow and spherical Brinkman regions acting at any point on ∂S are equal in magnitude and direction but of opposite sense. These interfacial conditions are consistent with those derived by Hou *et al.* (1989) in the limit as the solid volume fraction vanishes.

Using the transformations between cylindrical and spherical coordinates and between cylindrical and bispherical, given respectively by (4.1) and (5.1), it can be shown that the interfacial velocity and stress-traction conditions given by (8.1) provide the following six interfacial conditions on the spherical porous surface, ∂S, in terms of the spherical coordinate, ϕ:

$$Q(\operatorname{cosech}\alpha, \phi) = \tilde{Q}(\eta(\operatorname{cosech}\alpha, \phi), \alpha), \tag{8.2}$$

$$w(\operatorname{cosech}\alpha, \phi) = \tilde{w}(\eta(\operatorname{cosech}\alpha, \phi), \alpha), \tag{8.3}$$

$$U_0(\operatorname{cosech}\alpha, \phi) = \tilde{U}_0(\eta(\operatorname{cosech}\alpha, \phi), \alpha) + c_s\left(\frac{\cos\phi}{\sinh\alpha} + \coth\alpha\right), \tag{8.4}$$

$$U_2(\operatorname{cosech}\alpha, \phi) = \tilde{U}_2(\eta(\operatorname{cosech}\alpha, \phi), \alpha), \tag{8.5}$$

$$\frac{\sin\phi}{\sinh\alpha}\frac{\partial Q}{\partial \varrho}\bigg|_{\varrho=\operatorname{cosech}\alpha} + 2\frac{\partial U_0}{\partial \varrho}\bigg|_{\varrho=\operatorname{cosech}\alpha} = \left(\frac{\cosh\alpha\cos\phi + 1}{\cosh\alpha + \cos\phi} - \cosh\alpha\right)\left(\frac{\sin\phi}{\sinh\alpha}\frac{\partial \tilde{Q}}{\partial \xi}\bigg|_{\xi=\alpha} + 2\frac{\partial \tilde{U}_0}{\partial \xi}\bigg|_{\xi=\alpha}\right), \tag{8.6}$$

$$\frac{\sin\phi}{\sinh\alpha}\frac{\partial Q}{\partial \varrho}\bigg|_{\varrho=\operatorname{cosech}\alpha} + 2\frac{\partial U_2}{\partial \varrho}\bigg|_{\varrho=\operatorname{cosech}\alpha} = \left(\frac{\cosh\alpha\cos\phi + 1}{\cosh\alpha + \cos\phi} - \cosh\alpha\right)\left(\frac{\sin\phi}{\sinh\alpha}\frac{\partial \tilde{Q}}{\partial \xi}\bigg|_{\xi=\alpha} + 2\frac{\partial \tilde{U}_2}{\partial \xi}\bigg|_{\xi=\alpha}\right) + 2\,c_s\cos\phi, \tag{8.7}$$

where the quantities

$$\sin(\eta(\operatorname{cosech}\alpha, \phi)) = \frac{\sin\phi\sinh\alpha}{\cosh\alpha + \cos\phi} \quad \text{and} \quad \cos(\eta(\operatorname{cosech}\alpha, \phi)) = \frac{\cosh\alpha\cos\phi + 1}{\cosh\alpha + \cos\phi} \tag{8.8}$$

are used to replace $\sin\eta$ and $\cos\eta$ in the right-hand sides of (8.2)–(8.7) after making the substitution for the series solutions for $\tilde{Q}$, $\tilde{w}$, $\tilde{U}_0$ and $\tilde{U}_2$, given by (6.6)–(6.9). Refer to Appendix A for details on obtaining (8.2)–(8.7).

Upon making these substitutions, (8.2)–(8.7) express the six interfacial conditions on ∂S in terms that depend only on the spherical coordinate, ϕ, and the single parameter, α. In the light of the solutions for the flow in the spherical Brinkman and Stokes-flow regions, given, respectively, by (6.1)–(6.4) and (6.6)–(6.9), it follows that arguments of the respective Legendre polynomials associated with those solutions are $\cos\phi$, on the left-hand sides of (8.2)–(8.7) and $\cos(\eta(\operatorname{cosech}\alpha, \phi))$, given by (A27*a*,*b*), on the right-hand sides of (8.2)–(8.7). While the eigenfunctions $P_m(\cos\phi)$ (or $P'_m(\cos\phi)$ or $P''_m(\cos\phi)$) are mutually orthogonal to $P_n(\cos\phi)$ (or $P'_n(\cos\phi)$ or $P''_n(\cos\phi)$) on the left-hand sides of (8.2)–(8.7), they are not orthogonal to the eigenfunctions $P_n(\cos(\eta(\operatorname{cosech}\alpha, \phi)))$ (or $P'_m(\cos(\eta(\operatorname{cosech}\alpha, \phi)))$ or $P''_m(\cos(\eta(\operatorname{cosech}\alpha, \phi))))$ on the right-hand sides of (8.2)–(8.7). By forming the inner product of (8.2)–(8.7) with $P_m(\cos\phi)$ (or their derivatives with respect to $\cos\phi$), the infinite series on the left-hand sides of each of these equations will each reduce to a single term corresponding to the mth term in each series. On the other hand, the infinite series on the right-hand sides of each of these equations will not collapse but rather will transform into infinite series of inner products between $P_m(\cos\phi)$ and $P_n(\cos(\eta(\operatorname{cosech}\alpha, \phi)))$

(or their derivatives relative to their respective arguments), which themselves are independent of ϕ and depend parametrically only on α.

If the series solutions, given by (6.6)–(6.9), are truncated at N terms, then forming these inner products with each of the six interfacial conditions given above provides a system of $6N$ linear equations that involves recursive expressions on the left-hand side of each equation in terms of some combination of the unknown coefficients a_n, c_n, e_n and g_n and infinite series of inner products multiplying factors involving some combination of the first N unknown coefficients $\tilde{a}_n$, $\tilde{b}_n$, $\tilde{c}_n$, $\tilde{d}_n$, $\tilde{e}_n$, $\tilde{f}_n$, $\tilde{g}_n$ and $\tilde{h}_n$. These six recursion relations are given in Appendix B.

It should be noted that the interfacial conditions described in this section could also be recast in bispherical coordinates. The results described in the subsequent sections would be identical; however the subsequent $6N$ linear equations would take a different form. In particular, the linear equations would involve more difficult inner products to evaluate, and would therefore be more computationally cumbersome and time consuming. It is for this reason that in the final analysis, the calculations to determine the coefficients were carried out in terms of spherical rather than bispherical coordinates.

9. Drag force on the sphere and torque about the sphere centre

The hydrodynamic drag force, $\boldsymbol{F}^* = (F_x^*, F_y^*, F_z^*)$, exerted on the sphere and torque, $\boldsymbol{T}^* = (T_x^*, T_y^*, T_z^*)$, about the sphere centre are defined by the following integral expressions:

$$\boldsymbol{F}^* \equiv \int_{\partial S} \tilde{\boldsymbol{\sigma}}^*(\boldsymbol{x}^*)\cdot\boldsymbol{e}_\varrho \,\mathrm{d}A^* \quad \text{and} \quad \boldsymbol{T}^* \equiv \int_{\partial S} a\,\boldsymbol{e}_\varrho \times \left(\tilde{\boldsymbol{\sigma}}^*(\boldsymbol{x}^*)\cdot\boldsymbol{e}_\varrho\right) \mathrm{d}A^*.$$

The Cartesian components of these integrals are given, respectively, by

$$F_x^* = \tfrac{1}{2}\pi\mu\, Vc \int_{-1}^{1} \left(\tilde{Q}\,\frac{\partial r}{\partial \xi} - r\frac{\partial \tilde{Q}}{\partial \xi} - 2\frac{\partial \tilde{U}_0}{\partial \xi}\right)_{\xi=\alpha} \mathrm{d}\nu, \quad F_y^* = F_z^* = 0 \tag{9.1}$$

and

$$T_y^* = -\pi\mu\, Vc \,\mathrm{cosech}\,\alpha \int_{-1}^{1} \left(\frac{\partial r}{\partial \xi}\frac{\partial}{\partial \xi}\left(\tfrac{1}{2}z\tilde{Q} + \tilde{w}\right) - \frac{\partial z}{\partial \xi}\frac{\partial}{\partial \xi}\left(\tfrac{1}{2}r\tilde{Q} + \tilde{U}_0\right)\right)_{\xi=\alpha} \mathrm{d}\nu,$$
$$T_x^* = T_z^* = 0, \tag{9.2}$$

where $\nu = \cos\eta$ (Dean & O'Neill 1963). Using the exact series solutions, Dean & O'Neill (1963) and O'Neill (1964) analytically evaluated (9.1) and (9.2) for the cases of pure rotational motion ($V = c\,\Omega$) and pure translational motion ($V = U$) of a solid sphere in an otherwise quiescent fluid near a planar confining boundary. The dimensionless form of the exact series solutions corresponding to (9.1) and (9.2) are given, respectively, by

$$2^{-1/2} F_x^i = \frac{\beta_i \sinh\alpha}{6\,H(\epsilon_a)} \sum_{n=1}^{\infty} \left(n\,(n+1)\,\tilde{d}_n + \tilde{f}_{n-1}\right), \quad F_y = F_z = 0, \tag{9.3}$$

and

$$2^{1/2} T_y^i = \frac{\delta_i \sinh^2\alpha}{4\,H(\epsilon_a)} \sum_{n=1}^{\infty} \big(2n\,(n+1)\,\tilde{b}_n - (2n+1)\,(\tilde{e}_{n-1} + \tilde{f}_{n-1})$$
$$+ \coth\alpha\,(n\,(n+1)\,(\tilde{c}_n + \tilde{d}_n) + (\tilde{e}_{n-1} + \tilde{f}_{n-1}))\big), \quad T_x = T_z = 0, \tag{9.4}$$

for $i = t, r, s$ where $\beta_t = \delta_t = 1$, $\beta_r = \delta_r = -\sinh\alpha$, $\beta_s = -\tanh\alpha$, and $\delta_s = -2\sinh\alpha$, and the superscripts t, r, and s correspond, respectively, to pure translation, pure rotation, and uniform shear. In (9.3) and (9.4), the quantity $H(\epsilon_a)$ is defined as follows:

$$H(\epsilon_a) = \frac{2\,(1 - \epsilon_a \tanh(1/\epsilon_a))}{2 + 3\,\epsilon_a^2\,(1 - \epsilon_a \tanh(1/\epsilon_a))} \tag{9.5}$$

where $\epsilon_a^2 = (c/a)^2\epsilon^2$. Because c varies with d/a, so too does the dimensionless permeability, ϵ^2, if μ and K are held constant. It is therefore more convenient to express results in terms of ϵ_a^2, the dimensionless permeability based on sphere radius, a. In (9.3) and (9.4) the dimensionless force and torque components are defined relative to their dimensional counterparts according to

$$F_x^r = \frac{F_x^{*r}}{6\pi\mu\Omega a^2 H(\epsilon_a)}, \quad F_x^t = \frac{F_x^{*t}}{6\pi\mu U a H(\epsilon_a)}, \quad F_x^s = \frac{F_x^{*s}}{6\pi\mu\dot\gamma a d H(\epsilon_a)}$$
$$T_y^r = \frac{T_y^{*r}}{8\pi\mu\Omega a^3 H(\epsilon_a)}, \quad T_y^t = \frac{T_y^{*t}}{8\pi\mu U a^2 H(\epsilon_a)}, \quad T_y^s = \frac{T_y^{*s}}{4\pi\mu\dot\gamma a^3 H(\epsilon_a)}.$$

For a characteristic velocity, V, the terms in the denominator of the above six expressions for the dimensionless force and torque are the dimensional force, $6\pi\mu V a H(\epsilon_a)$, and torque, $8\pi\mu V a^2 H(\epsilon_a)$, about the sphere centre, experienced by a porous sphere in an unbounded fluid medium that is otherwise at rest (Debye & Bueche 1948).

10. Free motion of a neutrally buoyant sphere

In the case of a neutrally buoyant porous sphere in a uniform shear field bounded by a planar confining boundary, Ω and U cannot be specified independently. In order to obtain the rotational and translational speeds associated with the free motion of a neutrally buoyant sphere in a Stokes flow that decays to a uniform shear field in the far field, the sum of the externally applied viscous drag forces on the sphere, and the sum of the external torques about the sphere centre must vanish. Goldman *et al.* (1967) showed that for a neutrally buoyant sphere translating in the x-direction and rotating about the y-axis, these conditions can be satisfied simultaneously for Ω and U if we require that

$$\frac{\Omega}{\frac{1}{2}\dot\gamma} = \frac{2(d/a)F_x^s T_y^t - F_x^t T_y^s}{F_x^t T_y^r - F_x^r T_y^t}, \quad \frac{U}{d\dot\gamma} = \frac{\frac{1}{2}(a/d)F_x^r T_y^s - F_x^s T_y^r}{F_x^t T_y^r - F_x^r T_y^t}. \tag{10.1}$$

Thus the free motion of a neutrally buoyant porous sphere rotating and translating in a uniform shear field bounded by a rigid plane is fully characterized by Ω and U given by (10.1). Determination of these two quantities not only provides the free motion of a neutrally buoyant porous sphere, but also leads to the appropriate scaling of the dimensionless velocity and pressure fields associated with the three elemental problems we have considered such that linear superposition of the scaled solutions for a given value of $\dot\gamma$ provides the velocity and pressure fields for the neutrally buoyant case as well.

11. Results

The flow at a particular point in the two-dimensional parameter space (α, ϵ) for each of the three cases considered is uniquely determined by the eight sets of coefficients, $\{\tilde a_n, \tilde b_n, \tilde c_n, \tilde d_n, \tilde e_{n-1}, \tilde f_{n-1}, \tilde g_{n+1}, \tilde h_{n+1}\}$ for $n = 1, 2, \ldots$ in the Stokes-flow region and the

four sets of coefficients, $\{a_n, c_n, e_{n-1}, g_{n+1}\}$ for $n = 1, 2, \ldots$ in the spherical Brinkman region. In order to make this determination, we must first truncate the infinite series solutions for $\tilde{Q}$, $\tilde{W}$, $\tilde{U}_0$ and $\tilde{U}_2$ in the Stokes-flow region and for Q, W, U_0 and U_2 in the spherical Brinkman region, such as to retain only the leading N terms in each series. The $12N$ coefficients are then found that uniquely satisfy the $12N$ system of linear equations derived from the $3N$ recursion relations obtained from the no-slip boundary condition on the reference plane, P, given by (7.4)–(7.6), the $2N$ recursion relations derived from the continuity equation in the Stokes-flow region, given by (6.11) and (7.7), the N recursion relations derived from the continuity equation for the spherical Brinkman region, given by (6.5), and the $6N$ recursion relations (see Appendix B) obtained from the six interfacial boundary conditions on the spherical interfacial surface, ∂S, given by (B1)–(B6).

Since all of the series solutions are convergent, accuracy increased with increasing N. As expected, in order to achieve a given accuracy, a greater number of terms in the series solutions had to be retained for small values of α (corresponding to small clearances between the sphere and the reference plane, P) than for large values. However, as N increased, the determinant of the $12N \times 12N$ matrix associated with the $12N$ system of linear equations decreased. Using traditional numerical methods, the number of terms that could be retained in the series solutions was then limited by machine precision since increasing N above a certain threshold resulted in an ill-conditioned matrix as far as the precision of the calculations was concerned. Matrix inversion then resulted in the accumulation of significant numerical errors in the $12N$ coefficients. To obviate this limitation, all calculations were carried out using multiple precision. Furthermore, when assembling the $12N \times 12N$ matrix, all matrix elements were left in symbolic form or as rational fractions whenever possible, with conversion to their floating-point approximations being left as a final step before matrix inversion. When computing the series solutions for all of the results presented here, we set $N = 20$ and carried 50 digits of precision. Using these settings, the no-slip condition along the reference plane, P, the continuity equations throughout the Stokes-flow and spherical Brinkman regions, and the interfacial boundary conditions on the spherical interfacial surface, ∂S, were satisfied with an accuracy that exceeded machine precision. Because of the need for multiple-precision calculations and for symbolic manipulation of the $12N$ system of linear equations, all computations were performed using a symbolic algebra package (*Mathematica*, Wolfram Research, Inc.) on a MacBook Pro (Apple, Inc.).

It was noted, not surprisingly, that for a given point in the parameter space (α, ϵ), solutions for the case of uniform shear required retention of a greater number of terms to achieve a given accuracy than did solutions for the cases of pure translation and pure rotation. When calculating the drag force and torque on the porous sphere, we did not compute the coefficients for the case of uniform shear at each of the points in the parameter space considered since this would have required the retention of many more terms in the series solutions than were necessary in the other two cases if comparable accuracy was to be obtained. Instead, all of the information required to compute drag force and torque for the case of uniform shear is obtainable from the coefficients associated with the other two cases by invoking a quadrature method first conceived by Brenner (1964) and later implemented by Goldman (1966). There it was shown, through consideration of the stress-traction vector on the solid sphere surface, that for the case of uniform shear, the drag force on a solid sphere and the torque about the sphere centre could be determined from the coefficients of the pure translational and pure rotational problems, respectively. The same arguments

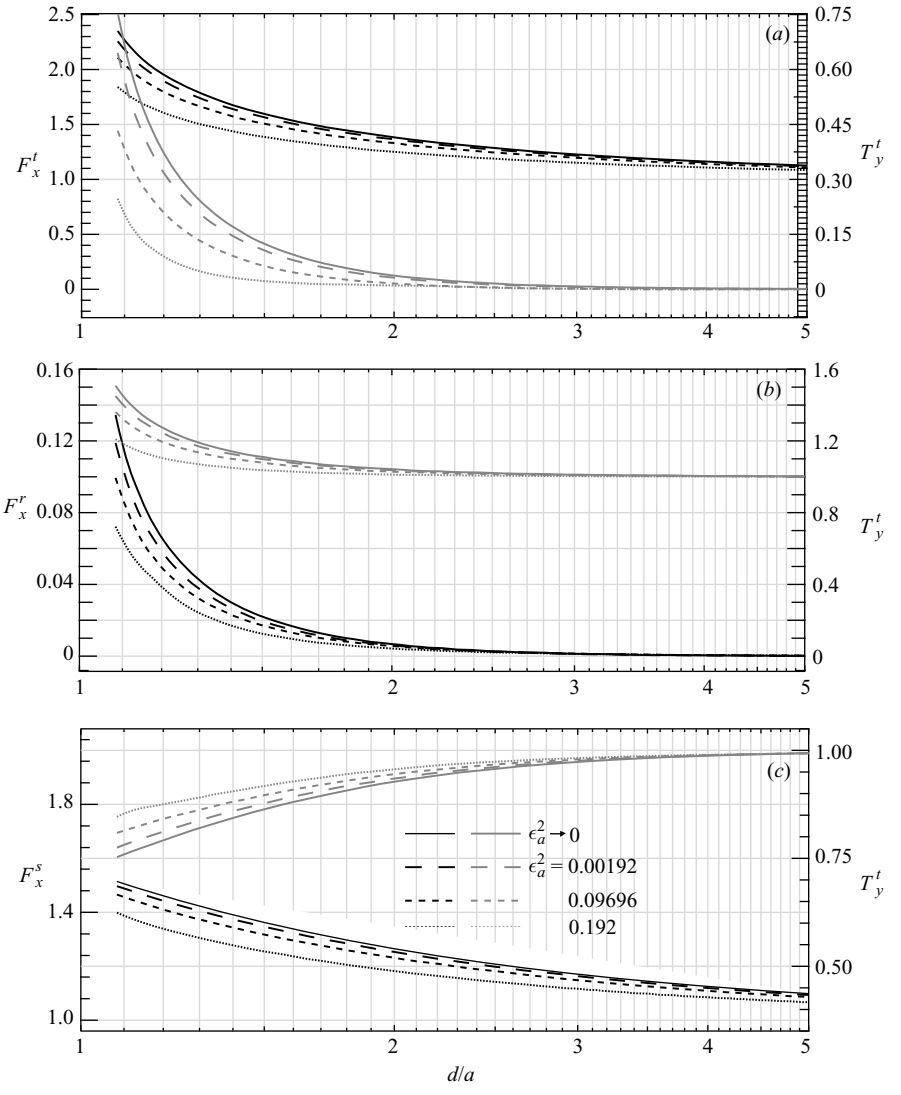

FIGURE 2. Variation, with respect to d/a, in the magnitudes of the dimensionless drag force on a porous sphere (black curves, left axis) and torque on a porous sphere about its centre (grey curves, right axis) if the sphere, having radius a and centred at a distance d above the reference plane, P, is (*a*) translating without rotation through an otherwise quiescent fluid, (*b*) rotating without translation through an otherwise quiescent fluid, or (*c*) stationary in a flow that decays to a uniform shear field in the far field. All cases are shown for the same three values of the dimensionless permeability, ϵ_a^2, and for a vanishing permeability (solid curves) when the porous sphere is replaced by a solid sphere.

apply to this problem, where the porous sphere is in proximity to the reference plane, P.

Figure 2 shows the magnitudes of the dimensionless drag force (black curves, left axis) and torque about the sphere centre (grey curves, right axis), on a porous sphere of radius a that is (*a*) purely translating, (*b*) purely rotating, and (*c*) stationary in a uniform shear field for various values of ϵ_a^2, as a function of the dimensionless distance, d/a, between the reference plane, P, and the sphere centre. Figure 3 shows

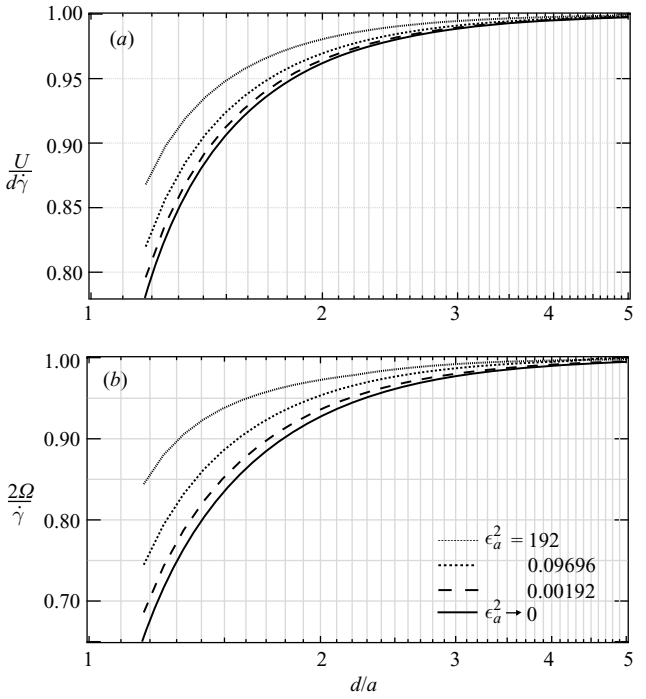

FIGURE 3. Variation, with respect to d/a, of the relative (a) translational speed, $U/(d\dot{\gamma})$, and (b) rotational speed, $2\Omega/\dot{\gamma}$, for the free motion of a neutrally buoyant porous sphere of radius a centred a distance d above the reference plane, P, that is convected through a Stokes flow, which decays to a uniform shear field in the far field. Results are shown for the same three values of ϵ_a^2 shown in figure 2. The curves in (a) represent the transformation between the translational speed of a porous sphere centred a distance d above the reference plane, P, and the translational speed, $d\dot{\gamma}$, a fluid particle would have, located a distance d above the plane, in a uniform shear field in the absence of the sphere. The curves in (b) represent the transformation between the rotational speed of that porous sphere and the constant solid-body rotation, $\dot{\gamma}/2$, that a fluid particle would have in a uniform shear field in the absence of the sphere.

the relative (a) translational and (b) rotational speeds for the free motion of a neutrally buoyant porous sphere in a uniform shear field, with the constant shear rate $\dot{\gamma}$ in the far field, as a function of d/a for various values of ϵ_a^2. The results are plotted for the dimensionless permeabilities of the porous sphere corresponding to $\epsilon_a^2 = 1.92 \times 10^{-1}$, 9.696×10^{-2}, 1.92×10^{-3}, and as $\epsilon_a^2 \to 0$. These three values correspond to dimensional hydraulic resistivity values of $K \approx 3.2 \times 10^7$, 3.2×10^8, 3.2×10^9 dyn s cm^{-4}, and as $K \to \infty$, respectively, for a viscosity $\mu = 0.012$ dyn s cm^{-2} and a sphere radius $a = 0.25$ μm. Similar values of permeability were considered by Davis (2001) to analyse the flow due to a porous sphere sedimenting towards a solid wall and by Damiano *et al.* (2004*a*) to analyse the motion of a solid sphere adjacent to a Brinkman half-space. In figures 2 and 3, the range of d/a shown corresponds to $\ln(3/2) \leqslant \alpha \leqslant \ln 10$ ($0.41 \lesssim \alpha \lesssim 2.3$). This range corresponds to a dimensionless minimal clearance between the sphere and the reference plane, P, of $0.08 \lesssim (d/a) - 1 \lesssim 4.05$, which, in terms of the dimensional parameters referenced above, corresponds to a minimal clearance range of $0.02 \lesssim d - a \lesssim 1.01$ μm.

The exact solution presented here is valid arbitrarily close to but not at the limit where the distance between the sphere and wall vanishes, i.e. for all values of $d/a > 1$.

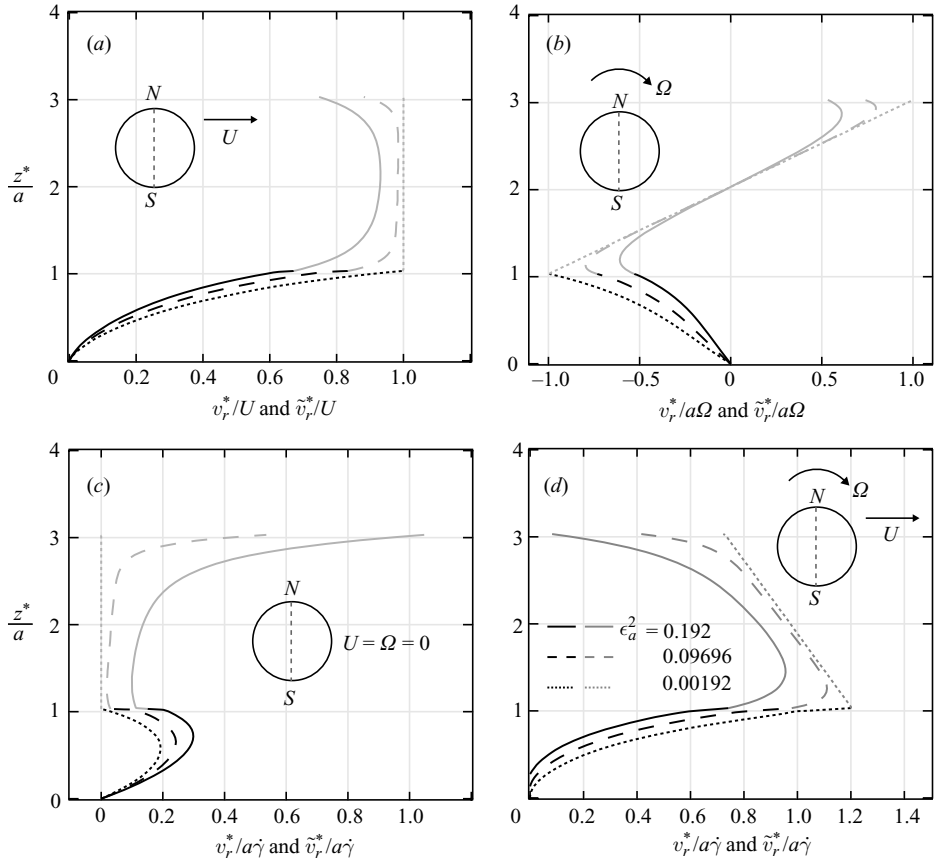

FIGURE 4. Dimensionless radial velocity profiles in the Stokes-flow region under the south pole (black curves), and in the spherical Brinkman region along the north–south axis, NS (the adjoining grey curves), for a porous sphere that is (*a*) purely translating, (*b*) purely rotating, (*c*) stationary in a Stokes flow that decays to a uniform shear field in the far field, and (*d*) neutrally buoyant and freely convected through a Stokes flow that decays to a uniform shear field in the far field. Results are shown for the same three non-zero values of ϵ_a^2 shown in figure 2. Note, the abscissa ranges vary, and the representation of the porous sphere in each panel is not shown to scale.

A singularity arises in our solution for the particular case of $d/a = 1$. To treat this case analytically, we could consider using the tangent-sphere coordinate system (Moon & Spencer 1961), which O'Neill (1968) employed when he considered a Stokes flow around a stationary sphere in contact with a plane in a linear shear field. Although our solution is valid arbitrarily close to but not at the limit where the distance between the sphere and wall vanishes, it nevertheless becomes computationally time consuming to compute solutions for values of $d/a <\sim 1.01$ (as this would require very high-precision calculations and a retention of a large number of terms in the infinite series solutions). For such small clearances between the sphere and the plane, an asymptotic analysis, similar to the approach taken by O'Neill & Stewartson (1967), would be much more practical. Such an analysis, however, is certainly beyond the scope of the present study.

Figure 4 shows the dimensionless radial velocity profiles as a function of the dimensionless distance, z^*/a, of the Stokes flow in the (x, z)-plane at $y = 0$ under

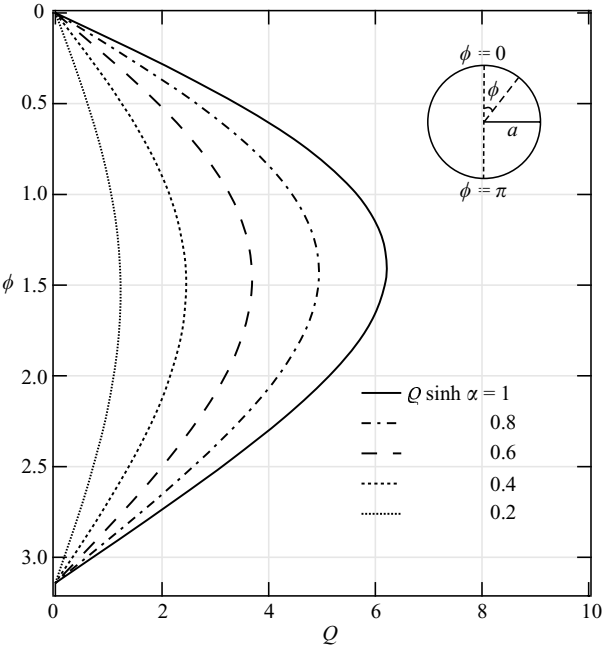

FIGURE 5. Dimensionless pressure variations inside a neutrally buoyant porous sphere along its interfacial surface, ∂S ($\varrho^*/a = 1$), and four equally spaced radial positions within the sphere arising from a Stokes flow generated by the free motion of the sphere in a flow regime that decays to a uniform shear field in the far field. The dimensionless permeability corresponds to $\epsilon_a^2 = 1.92 \times 10^{-3}$ and the minimal clearance between the sphere and the interfacial plane is as in figure 4.

the 'south pole' of the porous sphere (in black) and in the spherical Brinkman region along the 'north–south' axis (in grey) for the case of porous sphere that is (*a*) purely translating, (*b*) purely rotating, (*c*) stationary in a flow that decays to a uniform shear field in the far field, and (*d*) neutrally buoyant and freely convected along a flow that decays to a uniform shear field in the far field. Results are shown for the same three non-vanishing values of ϵ_a^2 shown in figures 2 and 3. The reference plane, P, is located at $z^*/a = 0$. It is clear from the radial velocity profiles that, as the sphere becomes less permeable, i.e. as ϵ_a^2 decreases, the motion of the fluid within the spherical Brinkman region approaches that of the rigid-body motion of a solid sphere.

Figure 5 shows the dimensionless pressure distribution, Q, in the (x, z)-plane at $y = 0$ inside a neutrally buoyant porous sphere along the spherical interfacial surface, ∂S ($\varrho^*/a = 1$) and at four equally spaced radial positions within the sphere, arising from a Stokes flow that decays to a uniform shear field in the far field. These distributions correspond to a dimensionless permeability corresponding to $\epsilon_a^2 = 0.192$. All calculations in figures 4 and 5 were performed for a minimal clearance of $\sim 1.032\,a$ ($\alpha = \ln(3.8) \approx 1.335$). The maximum pressure occurs along the interfacial surface, ∂S, of the porous sphere, where $\varrho^*/a = 1$, and decreases towards the interior of the sphere.

12. Applications in areas of engineering, environment, medicine and physiology

The hydrodynamic interactions of porous spheres with confining boundaries in a shear field is fundamental to the understanding of many phenomena involving the mechanics of porous agglomerates. The problem arises in numerous industrial and environmental processes. For example, porous pellets are used extensively in catalytic

reactors and it has been shown that convective transport in these particles might enhance effectiveness factors and improve selectivity of chemical reactors (Nir & Pismen 1977). Porous particles are frequently found in the atmosphere and in other environmental systems, where they are formed by vapour condensation–coagulation processes, processes that are affected by the hydrodynamic interactions with air (Pruppacher & Klett 1978).

Another application of this analysis is in the field of drug delivery and biomedicine. Inhalation aerosols have recently been developed as effective carriers of therapeutics for the treatment of respiratory inflammation, cystic fibrosis, and other lung disorders (Edwards *et al.* 1997; Tsapis *et al.* 2002). From figure 2, it is evident that the force coefficient increases much less rapidly with decreasing distance between a porous sphere ($\epsilon_a > 0$) and a rigid wall than if the sphere were solid ($\epsilon_a = 0$). The weaker hydrodynamic interaction in the case of a porous sphere would, in turn, influence the attachment rate of a porous sphere with the wall and would therefore also influence the drug transport properties of porous spheres relative to solid spheres. A major effort has been underway to develop porous particles of appropriate size that can prolong the residence of an administered drug in the airways and acini. Results of this analysis could provide quantitative guidance in this design process.

An example of a biological application of this analysis is in the area of inflammation. Numerous *in vitro* studies of leukocyte rolling dynamics in parallel-plate flow chambers have been undertaken to simulate early stages in the inflammatory response cascade in post-capillary venules. In these experiments, the cell culture medium, which is very well-approximated as Newtonian, is steadily perfused through a channel whose dimensions are large compared to the dimensions of the individual leukocytes suspended in the medium. Under typical flow-chamber conditions, the shear field is nearly uniform over length scales relevant to the leukocytes, which are either freely convected near, or undergoing adhesion-mediated rolling along, the bottom plate of the flow chamber. Typically, the freely convected motion of the leukocyte is modelled using the analysis of Goldman *et al.* (1967), where the leukocyte is approximated as a rigid smooth neutrally buoyant solid sphere freely convected near a planar confining boundary in a Stokes flow that decays to a uniform shear field far away from the leukocyte. The results of the present analysis, however, might be more appropriate in this context than the results of Goldman *et al.* (1967) in the light of the fact that activated leukocytes have a spiculated surface due to the erectile protrusions of microvilli. Furthermore, the surface of the leukocyte is also decorated with a glycocalyx, a dilute, macromolecular, carbohydrate-rich thin porous layer bound to the cell membrane. Since the ruffled surface of an activated leukocyte becomes spiculated, it is possible that the increased surface area of the cell (relative to a sphere of the same diameter as the leukocyte) might produce troughs (surrounded by pillars of microvilli) that are filled with glycocalyx. Collectively, then, the surface topology (due to microvilli) and the surface-bound glycocalyx might behave as a porous medium, and the system as a whole, then, might better be approximated as a solid sphere encased in a porous layer rather than as a solid sphere with a smooth surface. Although this analysis does not treat the problem of a solid sphere lined with a thin porous layer, it can, nevertheless, be applicable to that problem whenever the characteristic exponential decay depth, $(\mu/K)^{1/2}$, into the porous sphere (which is characteristic of the depth of flow penetration into a porous medium) is small compared with the thickness of a porous layer encasing a solid sphere. If this condition is met, then, from a hydrodynamical point of view, there would be little difference between a sphere that is entirely porous and one that is solid but encased in

a thin porous layer; in this case, the analysis presented here would be applicable. If the microvilli are on the order of 300–500 nm in length (Zhao, Chien & Weinbaum 2001) and the glycocalyx is conservatively 100–200 nm in thickness†, then this structure could effectively result in a vanishing fluid shear rate on the cell body, provided the hydraulic resistivity is sufficiently high. Based on the mechanics of red and white blood cells and the recovery time of the glycocalyx after compression by passing white blood cells in capillaries (Vink & Duling 1996; Feng & Weinbaum 2000; Damiano & Stace 2002; 2005; Weinbaum *et al.* 2003), a value of K between 10^{-11} and 10^{-10} dyn s cm^{-4} is a reasonable estimate for the hydraulic resistivity of the endothelial glycocalyx. For a viscosity, $\mu = 0.012$ dyn s cm^{-2}, corresponding to blood plasma, and a characteristic length scale of $a = 0.5$ μm, a value of ϵ_a that is between 0.007 and 0.02 might be a reasonable estimate for the leukocyte glycocalyx on mammalian microvessels.

Yet another application of this analysis is in the area of biophysics. In particular, ultrasensitive molecular force probe instruments have recently been developed (Wong 2006; Halvorsen 2007; Wong, Heinrich & Evans 2004; Heinrich *et al.* 2008) that use a laser trap to apply and measure piconewton forces exerted on a potential-confined micron-sized spherical glass bead. Typically, the bead is functionalized with biomolecules, such as immunological adhesion molecules. The reactive substrate (which might consist of counterligands to the adhesion molecule receptors adsorbed to the surface of the bead) can be adsorbed to the surface of a cover slip. Nanometre-sized three-dimensional displacements between the bead and the substrate are monitored using optical interferometry and recorded using high-speed video processing. Calibration of these instruments can be achieved through a variety of techniques (Wong 2006; Halvorsen 2007; Wong *et al.* 2004; Wong & Halvorsen 2006; Heinrich *et al.* 2007), but one involves optically trapping the glass bead within a viscous shear field induced by moving the fluid-filled chamber relative to the optical trap (Halvorsen 2007). By precisely measuring the bead displacement within the trap under the known hydrodynamic drag force, the strength of the optical trap can be estimated. If the bead is brought into close proximity with the cover slip in this experiment, a linear superposition of the analyses of Dean & O'Neill (1964) and Goren & O'Neill (1971) could be used to detail the hydrodynamic interaction of a rotating functionalized smooth glass bead in a shear field, with the reactive substrate on the cover slip, as a function of distance between the sphere and the substrate. On the other hand, if the surface of the glass bead were coated with a polyethylene glycol (PEG) surface layer and functionalized with adhesion receptors (or counterligands), the functionalized PEG-coated bead might better be approximated as a solid sphere encased in a porous layer rather than as a solid sphere with a smooth functionalized surface. In this case, as before, the analysis presented here might prove useful in estimating the drag force on the PEG-coated glass bead, so long as the characteristic decay length, $(\mu/K)^{1/2}$, associated with the PEG layer, is small compared with the thickness of the PEG layer encasing the glass bead. In this case, the instrument could be used to characterize the hydrodynamic effects of an adsorbed porous PEG layer on the functionalized surface of a glass bead that is brought into close proximity with the reactive substrate on the cover slip. Such a model experimental system could be used to investigate how a mucopolysaccharide surface layer, such as the surface glycocalyx on a spheroidal leukocyte or the PEG-coated layer on a spherical drug delivery vesicle, interferes with, or possibly enhances, adhesion events with a reactive substrate.

† On endothelial cells of mammalian microvessels the glycocalyx is $\sim$ 500 nm in thickness (Vink & Duling 1996; Smith *et al.* 2003; Damiano, Long & Smith 2004*b*; Long *et al.* 2004).

13. Extensions of the present analysis

We are currently extending the analysis to study the motion of a porous sphere parallel to a Brinkman half-space. Because the governing differential equations and the boundary and interfacial conditions are linear, the solution to this problem can be obtained by a linear superposition of the solution presented here with the solution describing the motion of a solid sphere adjacent to a Brinkman half-space, as described by Damiano *et al.* (2004*a*). Such an analysis would be valid for arbitrary values of ϵ_a in the porous sphere and asymptotically small values of ϵ_a in the Brinkman half-space. With considerably more effort, one could extend the analysis presented here to study the motion of a porous sphere in a Stokes flow parallel to and between two parallel planar confining boundaries. Whereas the dependent variables inside the porous sphere would be expressed in spherical coordinates, the dependent variables in the Stokes-flow region would be expressed in cylindrical rather than bispherical coordinates. Although cylindrical and spherical coordinates do not share a common coordinate surface on which to evaluate the interfacial conditions on the surface of the porous sphere, the collocation technique described by Ganatos, Pfeffer & Weinbaum (1980) could be used to enforce the interfacial conditions. A further extension could then be made to analyse the motion of a porous sphere in a Stokes flow parallel to and between two parallel Brinkman half-spaces, which are separated by a finite distance and extend semi-infinitely in opposite directions. Because the Brinkman equations are separable in cylindrical coordinates, the dependent variables in the Stokes-flow region and Brinkman half-spaces would be expressed in cylindrical coordinates such that the interfacial conditions between the Stokes-flow region and Brinkman half-spaces could be evaluated analytically.

Partial support for this work was contributed by the National Science Foundation, BES-0093985. We would like to thank Ken Halvorsen for useful discussions and Evan Evans for planting the seeds of suggestion that we take this problem on.

Appendix A. Spherical coordinate representation of the interfacial velocity and stress conditions

In terms of scalar cylindrical components, the interfacial velocity and stress-traction conditions, given by (8.1*a*,*b*), are expressed in cylindrical coordinates (r^*, θ, z^*) by

$$v_r^* = \tilde{v}_r^*, \quad v_\theta^* = \tilde{v}_\theta^*, \quad v_z^* = \tilde{v}_z^*, \quad \forall\ (r^*, \theta, z^*) \in \partial S, \tag{A1}$$

$$\left(-\frac{p^*}{\mu} + 2\frac{\partial v_r^*}{\partial r^*}\right)\sin\phi + \left(\frac{\partial v_r^*}{\partial z^*} + \frac{\partial v_z^*}{\partial r^*}\right)\cos\phi = \left(-\frac{\tilde{p}^*}{\mu} + 2\frac{\partial \tilde{v}_r^*}{\partial r^*}\right)\sin\phi + \left(\frac{\partial \tilde{v}_r^*}{\partial z^*} + \frac{\partial \tilde{v}_z^*}{\partial r^*}\right)\cos\phi, \quad \forall\ (r^*, \theta, z^*) \in \partial S, \tag{A2}$$

$$\left(\frac{\partial v_\theta^*}{\partial r^*} - \frac{v_\theta^*}{r^*} + \frac{1}{r^*}\frac{\partial v_r^*}{\partial \theta^*}\right)\sin\phi + \left(\frac{\partial v_\theta^*}{\partial z^*} + \frac{1}{r^*}\frac{\partial v_z^*}{\partial \theta}\right)\cos\phi = \left(\frac{\partial \tilde{v}_\theta^*}{\partial r^*} - \frac{\tilde{v}_\theta^*}{r^*} + \frac{1}{r^*}\frac{\partial \tilde{v}_r^*}{\partial \theta^*}\right)\sin\phi + \left(\frac{\partial \tilde{v}_\theta^*}{\partial z^*} + \frac{1}{r^*}\frac{\partial \tilde{v}_z^*}{\partial \theta}\right)\cos\phi, \quad \forall\ (r^*, \theta, z^*) \in \partial S, \tag{A3}$$

$$\left(-\frac{p^*}{\mu}+2\frac{\partial v_z^*}{\partial z^*}\right)\cos\phi+\left(\frac{\partial v_r^*}{\partial z^*}+\frac{\partial v_z^*}{\partial r^*}\right)\sin\phi$$
$$=\left(-\frac{\tilde{p}^*}{\mu}+2\frac{\partial \tilde{v}_z^*}{\partial z^*}\right)\cos\phi+\left(\frac{\partial \tilde{v}_r^*}{\partial z^*}+\frac{\partial \tilde{v}_z^*}{\partial r^*}\right)\sin\phi,\quad \forall\ (r^*,\theta,z^*)\in\partial S, \tag{A4}$$

where the left-hand sides of (A2)–(A4) correspond, respectively, to the cylindrical components (r^*,θ,z^*) of the quantity $\boldsymbol{\sigma}^*(\boldsymbol{x}^*)\cdot(\sin\phi\,\boldsymbol{e}_r+\cos\phi\,\boldsymbol{e}_z)/\mu$.

The coordinate surface $\varrho=a/c>0$ corresponds to the locus of points that lie on the spherical interfacial surface, ∂S. Using the transformation between the dimensionless cylindrical coordinates (r,θ,z) and spherical coordinates (ϱ,θ,ϕ), given by (4.1), and the chain rule of differentiation, the dimensionless counterparts to (A1)–(A4) are respectively expressed in terms of the dimensionless spherical coordinates as

$$v_r=\tilde{v}_r,\quad v_\theta=\tilde{v}_\theta,\quad v_z=\tilde{v}_z,\quad \forall\ (\theta,\phi)\in\varrho=a/c, \tag{A5a–c}$$

$$-p\sin\phi+(1+\sin^2\phi)\frac{\partial v_r}{\partial\varrho}+\sin\phi\cos\phi\left(\frac{\partial v_z}{\partial\varrho}+\frac{1}{\varrho}\frac{\partial v_r}{\partial\phi}\right)+\frac{\cos^2\phi}{\varrho}\frac{\partial v_z}{\partial\phi}$$
$$=-\tilde{p}\sin\phi+(1+\sin^2\phi)\frac{\partial \tilde{v}_r}{\partial\varrho}+\sin\phi\cos\phi\left(\frac{\partial \tilde{v}_z}{\partial\varrho}+\frac{1}{\varrho}\frac{\partial \tilde{v}_r}{\partial\phi}\right)+\frac{\cos^2\phi}{\varrho}\frac{\partial \tilde{v}_z}{\partial\phi},$$
$$\forall\ (\theta,\phi)\in\varrho=a/c, \tag{A6}$$

$$\frac{\partial v_\theta}{\partial\varrho}+\frac{1}{\varrho}\left(\frac{\partial v_r}{\partial\theta}-v_\theta+\cot\phi\frac{\partial v_z}{\partial\theta}\right)=\frac{\partial \tilde{v}_\theta}{\partial\varrho}+\frac{1}{\varrho}\left(\frac{\partial \tilde{v}_r}{\partial\theta}-\tilde{v}_\theta+\cot\phi\frac{\partial \tilde{v}_z}{\partial\theta}\right),$$
$$\forall\ (\theta,\phi)\in\varrho=a/c, \tag{A7}$$

$$-p\cos\phi+(1+\cos^2\phi)\frac{\partial v_z}{\partial\varrho}+\sin\phi\cos\phi\left(\frac{\partial v_r}{\partial\varrho}-\frac{1}{\varrho}\frac{\partial v_z}{\partial\phi}\right)-\frac{\sin^2\phi}{\varrho}\frac{\partial v_r}{\partial\phi}$$
$$=-\tilde{p}\cos\phi+(1+\cos^2\phi)\frac{\partial \tilde{v}_z}{\partial\varrho}+\sin\phi\cos\phi\left(\frac{\partial \tilde{v}_r}{\partial\varrho}-\frac{1}{\varrho}\frac{\partial \tilde{v}_z}{\partial\phi}\right)-\frac{\sin^2\phi}{\varrho}\frac{\partial \tilde{v}_r}{\partial\phi},$$
$$\forall\ (\theta,\phi)\in\varrho=a/c. \tag{A8}$$

Since, according to (A5*a–c*), the three velocity components are continuous across ∂S, and since the θ- and ϕ-coordinate lines both lie on ∂S, all θ- and ϕ-derivatives of the velocity components must also be continuous across ∂S. Thus, the interfacial conditions associated with the three components of the stress-traction vector, given by (A6)–(A8), reduce to

$$-p\sin\phi+(1+\sin^2\phi)\frac{\partial v_r}{\partial\varrho}+\sin\phi\cos\phi\frac{\partial v_z}{\partial\varrho}$$
$$=-\tilde{p}\sin\phi+(1+\sin^2\phi)\frac{\partial \tilde{v}_r}{\partial\varrho}+\sin\phi\cos\phi\frac{\partial \tilde{v}_z}{\partial\varrho},\ \forall\ (\theta,\phi)\in\varrho=a/c, \tag{A9}$$

$$\frac{\partial v_\theta}{\partial\varrho}=\frac{\partial \tilde{v}_\theta}{\partial\varrho},\quad \forall\ (\theta,\phi)\in\varrho=a/c, \tag{A10}$$

$$-p\cos\phi + (1+\cos^2\phi)\frac{\partial v_z}{\partial \varrho} + \sin\phi\cos\phi\frac{\partial v_r}{\partial \varrho}$$
$$= -\tilde{p}\cos\phi + (1+\cos^2\phi)\frac{\partial \tilde{v}_z}{\partial \varrho} + \sin\phi\cos\phi\frac{\partial \tilde{v}_r}{\partial \varrho}, \forall\ (\theta,\phi) \in \varrho = a/c. \quad \text{(A11)}$$

Subtracting the product of $\sin\phi$ and (A11) from the product of $\cos\phi$ and (A9) provides

$$\cos\phi\frac{\partial v_r}{\partial \varrho} - \sin\phi\frac{\partial v_z}{\partial \varrho} = \cos\phi\frac{\partial \tilde{v}_r}{\partial \varrho} - \sin\phi\frac{\partial \tilde{v}_z}{\partial \varrho}, \quad \forall\ (\theta,\phi) \in \varrho = a/c. \quad \text{(A12)}$$

Using, again, the transformation between the dimensionless cylindrical coordinates (r,θ,z) and spherical coordinates (ϱ,θ,ϕ), given by (4.1), and the chain rule of differentiation, the dimensionless counterpart to the continuity equation, given by (3.4), is expressed in terms of the dimensionless spherical coordinates as

$$\left(\sin\phi\frac{\partial}{\partial \varrho} + \frac{\cos\phi}{\varrho}\frac{\partial}{\partial\phi}\right)v_r + \frac{1}{\varrho\sin\phi}\left(v_r + \frac{\partial v_\theta}{\partial\theta}\right) + \left(\cos\phi\frac{\partial}{\partial \varrho} - \frac{\sin\phi}{\varrho}\frac{\partial}{\partial\phi}\right)v_z = 0. \quad \text{(A13)}$$

Evaluating (A13) on each side of ∂S, and taking account of the result that all three velocity components and all θ- and ϕ-derivatives of the velocity components are continuous across ∂S, it is evident that

$$\sin\phi\frac{\partial v_r}{\partial \varrho} + \cos\phi\frac{\partial v_z}{\partial \varrho} = \sin\phi\frac{\partial \tilde{v}_r}{\partial \varrho} + \cos\phi\frac{\partial \tilde{v}_z}{\partial \varrho}, \quad \forall\ (\theta,\phi) \in \varrho = a/c. \quad \text{(A14)}$$

Subtracting the product of $\sin\phi$ and (A12) from the product of $\cos\phi$ and (A14) provides

$$\frac{\partial v_z}{\partial \varrho} = \frac{\partial \tilde{v}_z}{\partial \varrho}, \quad \forall\ (\theta,\phi) \in \varrho = a/c. \quad \text{(A15)}$$

Using (A15) in either of (A12) or (A14) provides

$$\frac{\partial v_r}{\partial \varrho} = \frac{\partial \tilde{v}_r}{\partial \varrho}, \quad \forall\ (\theta,\phi) \in \varrho = a/c. \quad \text{(A16)}$$

Finally, using (A15) and (A16) in either (A9) or (A11) establishes the continuity in the pressure across ∂S. Thus, (A5*a–c*), (A10), (A15), and (A16) constitute the six interfacial conditions that satisfy (8.1*a,b*).

Using the continuity in the r and θ velocity components across ∂S, given by (A5*a,b*), and the continuity in the velocity gradients across ∂S, given by (A10) and (A16), we arrive at the following four conditions, which are independent of θ:

$$\frac{v_r}{\cos\theta} \pm \frac{v_\theta}{\sin\theta} = \frac{\tilde{v}_r}{\cos\theta} \pm \frac{\tilde{v}_\theta}{\sin\theta}, \quad \forall\ \phi \in \varrho = a/c, \quad \text{(A17)}$$

$$\frac{1}{\cos\theta}\frac{\partial v_r}{\partial \varrho} \pm \frac{1}{\sin\theta}\frac{\partial v_\theta}{\partial \varrho} = \frac{1}{\cos\theta}\frac{\partial \tilde{v}_r}{\partial \varrho} \pm \frac{1}{\sin\theta}\frac{\partial \tilde{v}_\theta}{\partial \varrho}, \quad \forall\ \phi \in \varrho = a/c. \quad \text{(A18)}$$

Substituting the decoupling relations for the pressure and velocity components associated with the flow in the spherical Brinkman region, given by (3.9) and (3.10), and in the Stokes-flow region, given by (5.5) and (5.6), into (A17) and (A18), and using (A5*c*), we find that the three components of the velocity vector, the three components

of the stress-traction vector, and the pressure will all be continuous across ∂S if

$$Q = \tilde{Q}, \quad w = \tilde{w}, \quad U_0 = \tilde{U}_0 + c_s \left(\frac{a}{c} \cos\phi + \frac{d}{c} \right), \quad U_2 = \tilde{U}_2, \quad \forall\ \phi \in \varrho = a/c, \tag{A19}$$

$$\frac{a}{c} \sin\phi \frac{\partial Q}{\partial \varrho} + 2 \frac{\partial U_2}{\partial \varrho} = \frac{a}{c} \sin\phi \frac{\partial \tilde{Q}}{\partial \varrho} + 2 \frac{\partial \tilde{U}_2}{\partial \varrho}, \quad \forall\ \phi \in \varrho = a/c, \tag{A20}$$

$$\frac{a}{c} \sin\phi \frac{\partial Q}{\partial \varrho} + 2 \frac{\partial U_0}{\partial \varrho} = \frac{a}{c} \sin\phi \frac{\partial \tilde{Q}}{\partial \varrho} + 2 \frac{\partial \tilde{U}_0}{\partial \varrho} + 2 c_s \cos\phi, \quad \forall\ \phi \in \varrho = a/c. \tag{A21}$$

Note, that while (A20) and (A21) ensure that (A18), and therefore (A10) and (A16), are identically satisfied on ∂S, it is the jump condition derived from the continuity equation evaluated on ∂S, given by (A14), that, along with (A19)–(A21), ensures that (A15) is identically satisfied on ∂S.

The right-hand sides of (A19)–(A21) can be written, with the aid of (6.6)–(6.9), in terms of bispherical coordinates $(\eta, \xi = \alpha)$ evaluated on the spherical interfacial surface, ∂S. Combining (4.1) and (5.1) and using the chain rule of differentiation, the derivatives with respect to ϱ that appear in (A20) and (A21) can be expressed in terms of bispherical coordinates. In particular, the coordinate transformations $\varrho = \varrho(\eta, \xi)$ and $\phi = \phi(\eta, \xi)$ are given by

$$\varrho = \frac{\left(\sin^2\eta + (\sinh\xi - \coth\alpha(\cosh\xi - \cos\eta))^2 \right)^{1/2}}{\cosh\xi - \cos\eta}, \tag{A22}$$

$$\phi = \tan^{-1} \left(\frac{\sin\eta\ \sinh\alpha}{\cos\eta \cosh\alpha - \cosh(\xi - \alpha)} \right), \tag{A23}$$

from which it can be deduced that

$$\left. \frac{\partial}{\partial \varrho} \right|_{\varrho = a/c} = (\cos\eta - \cosh\alpha) \left. \frac{\partial}{\partial \xi} \right|_{\xi = \alpha} \tag{A24}$$

on the spherical interfacial surface, ∂S, where

$$\varrho = \frac{a}{c} = \frac{1}{\sinh\alpha} = \operatorname{cosech}\alpha \qquad \text{and} \qquad \xi = \alpha. \tag{A25}$$

On the other hand, the inverse coordinate transformation, $\eta = \eta(\varrho, \phi)$, when evaluated on the interfacial surface, ∂S, is found from (4.1) and (5.1) to be

$$\eta(\operatorname{cosech}\alpha, \phi) = \tan^{-1} \left(\frac{\sin\phi \sinh\alpha}{\cosh\alpha \cos\phi + 1} \right), \tag{A26}$$

where

$$\sin(\eta(\operatorname{cosech}\alpha, \phi)) = \frac{\sin\phi \sinh\alpha}{\cosh\alpha + \cos\phi}, \quad \cos(\eta(\operatorname{cosech}\alpha, \phi)) = \frac{\cosh\alpha \cos\phi + 1}{\cosh\alpha + \cos\phi}. \tag{A27a,b}$$

Using (A27*b*) in (A24) and then (A24) in (A20) and (A21) provides the expressions for the six interfacial conditions on ∂S in terms of spherical coordinates given by (8.2)–(8.7).

Appendix B. Recursion relations for the interfacial conditions on the sphere surface

After substituting Q, w, U_0, U_2, $\tilde{Q}$, $\tilde{w}$, $\tilde{U}_0$ and $\tilde{U}_2$, given by (6.1)–(6.4) and (6.6)–(6.9), into (8.2)–(8.7), and then forming the inner product of (8.2) and (8.3) with $P'_m(\cos\phi)$, (8.4) and (8.6) with $P_m(\cos\phi)$, and (8.5) and (8.7) with $P''_m(\cos\phi)$, we obtain, after making use of certain recursive and orthogonality properties of the Legendre polynomials, the following recursion relations for the six interfacial conditions on the spherical surface, ∂S:

$$\sinh^{n+2}\alpha \sum_{m=1}^{\infty} Q_{mn} \left\{ \tilde{c}_m \cosh\left(m+\tfrac{1}{2}\right)\alpha + \tilde{d}_m \sinh\left(m+\tfrac{1}{2}\right)\alpha \right\} = \frac{2n(n+1)}{2n+1} c_n, \qquad n = 1, 2, \ldots, \tag{B1}$$

$$\begin{aligned} &\sinh^{n+2}\alpha \sum_{m=1}^{\infty} Q_{mn} \left\{ \tilde{a}_m \cosh\left(m+\tfrac{1}{2}\right)\alpha + \tilde{b}_m \sinh\left(m+\tfrac{1}{2}\right)\alpha \right\} + \frac{n(n-1)(n+1)}{(2n-1)(2n+1)} c_{n-1} \\ &+ \frac{n(n+1)}{(2n+1)} c_n \coth\alpha + \frac{n(n+1)(n+2)}{(2n+1)(2n+3)} \left(\frac{1}{\sinh^2\alpha} + 2(2n+3)\epsilon^2 \right) c_{n+1} \\ &- \frac{2n(n+1)}{2n+1} I_{n+1/2}(1/(\epsilon \sinh\alpha))\, a_n \sinh^{n+1/2}\alpha = \begin{cases} -\frac{4}{3} c_r \sinh\alpha, & \text{if } n = 1 \\ 0, & \text{if n = 2, 3, \ldots,} \end{cases} \end{aligned} \tag{B2}$$

$$\begin{aligned} &\sinh^{n+1}\alpha \sum_{m=0}^{\infty} U_{0_{mn}} \left\{ \tilde{e}_m \cosh\left(m+\tfrac{1}{2}\right)\alpha + \tilde{f}_m \sinh\left(m+\tfrac{1}{2}\right)\alpha \right\} \\ &- \frac{n(n-1)}{(2n-1)(2n+1)} \left(1 + 4(n-1)\epsilon^2 \sinh^2\alpha\right) c_{n-1} \\ &+ \frac{(n+1)(n+2)}{(2n+1)(2n+3)} \left(\frac{1}{\sinh^2\alpha} + 2\frac{3n+4}{n+2}\epsilon^2 \right) c_{n+1} \\ &- \frac{2}{2n+1} I_{n+1/2}(1/(\epsilon \sinh\alpha))\, e_n \sinh^{n+1/2}\alpha = \begin{cases} -4\,(2\,c_t - c_s \coth\alpha), & \text{if } n = 0 \\ -\frac{4}{3}(2\,c_r - c_s)\sinh\alpha, & \text{if } n = 1 \\ 0, & \text{if n = 2, 3, \ldots,} \end{cases} \end{aligned} \tag{B3}$$

$$\begin{aligned} &\sinh^{n+3}\alpha \sum_{m=2}^{\infty} U_{2_{mn}} \left\{ \tilde{g}_m \cosh\left(m+\tfrac{1}{2}\right)\alpha + \tilde{h}_m \sinh\left(m+\tfrac{1}{2}\right)\alpha \right\} \\ &+ \frac{n(n-1)(n+1)(n+2)}{(2n-1)(2n+1)} c_{n-1} \\ &- \frac{n(n-1)(n+1)(n+2)}{(2n+1)(2n+3)} \left(\frac{1}{\sinh^2\alpha} + 2(2n+3)\epsilon^2 \right) c_{n+1} \\ &- \frac{2n(n-1)(n+1)(n+2)}{2n+1} I_{n+1/2}(1/(\epsilon \sinh\alpha))\, g_n \sinh^{n+1/2}\alpha = 0, \quad n = 2, 3, \ldots, \end{aligned} \tag{B4}$$

$$\sinh^{n-2}\alpha \sum_{m=0}^{\infty} S_{0_{mn}} \psi_m \sinh\left(m+\tfrac{1}{2}\right)\alpha$$
$$-\frac{n(n-1)}{(2n-1)(2n+1)}\left(\frac{1}{\sinh^2\alpha}+4(n-1)(n-2)\epsilon^2\right)\frac{c_{n-1}}{\sinh^2\alpha}$$
$$+\frac{(n+1)(n+2)}{(2n+1)(2n+3)}\left(\frac{1}{\sinh^2\alpha}+2n\frac{3n+4}{n+2}\epsilon^2\right)c_{n+1}$$
$$-\frac{2}{2n+1}\left\{n\, I_{n+1/2}(1/(\epsilon\sinh\alpha))+\frac{I_{n+3/2}(1/(\epsilon\sinh\alpha))}{\epsilon\sinh\alpha}\right\} e_n \sinh^{n+1/2}\alpha$$
$$=\begin{cases}\frac{4}{3}(2c_r-c_s), & \text{if } n=1\\ 0, & \text{if } n=0,2,3,\ldots,\end{cases} \tag{B5}$$

$$\sinh^{n}\alpha \sum_{m=2}^{\infty} S_{2_{mn}} \chi_m \sinh\left(m+\tfrac{1}{2}\right)\alpha$$
$$-\frac{n(n-1)(n+1)(n+2)}{(2n-1)(2n+1)}c_{n-1}$$
$$-\frac{n(n-1)(n+1)(n+2)}{(2n+1)(2n+3)}\left(\frac{1}{\sinh^2\alpha}+2n(2n+3)\epsilon^2\right)c_{n+1}$$
$$-\frac{2n(n-1)(n+1)(n+2)}{2n+1}\left\{n\, I_{n+1/2}(1/(\epsilon\sinh\alpha))+\frac{I_{n+3/2}(1/(\epsilon\sinh\alpha))}{\epsilon\sinh\alpha}\right\} g_n \sinh^{n+1/2}\alpha$$
$$=0, \quad n=2,3,\ldots. \tag{B6}$$

The inner products, Q_{mn}, $U_{0_{mn}}$, $U_{2_{mn}}$, $S_{0_{mn}}$, $S_{2_{mn}}$, are defined as

$$Q_{mn}=\int_{-1}^{1}\frac{1-\nu^2}{(\cosh\alpha+\nu)^{3/2}}P_m'\left(\frac{\nu\cosh\alpha+1}{\cosh\alpha+\nu}\right)P_n'(\nu)\,\mathrm{d}\nu,$$

$$U_{0_{mn}}=\int_{-1}^{1}\frac{1}{(\cosh\alpha+\nu)^{1/2}}P_m\left(\frac{\nu\cosh\alpha+1}{\cosh\alpha+\nu}\right)P_n(\nu)\,\mathrm{d}\nu,$$

$$U_{2_{mn}}=\int_{-1}^{1}\frac{(1-\nu^2)^2}{(\cosh\alpha+\nu)^{5/2}}P_m''\left(\frac{\nu\cosh\alpha+1}{\cosh\alpha+\nu}\right)P_n''(\nu)\,\mathrm{d}\nu,$$

$$S_{0_{mn}}=\int_{-1}^{1}(\cosh\alpha+\nu)^{1/2}P_m\left(\frac{\nu\cosh\alpha+1}{\cosh\alpha+\nu}\right)P_n(\nu)\,\mathrm{d}\nu,$$

$$S_{2_{mn}}=\int_{-1}^{1}\frac{(1-\nu^2)^2}{(\cosh\alpha+\nu)^{3/2}}P_m''\left(\frac{\nu\cosh\alpha+1}{\cosh\alpha+\nu}\right)P_n''(\nu)\,\mathrm{d}\nu,$$

where the substitution $\nu=\cos\phi$ was made, and the primes denote differentiation of the Legendre polynomials with respect to their arguments. The quantities ψ_m, and χ_m in (B5) and (B6) are defined as

$$\psi_m = \frac{m(m-1)(m-2)}{4\,(2m-1)}\,(\cosh 2\alpha - \kappa_m \sinh 2\alpha)\,\tilde{c}_{m-2}$$
$$+\left(\frac{m(m-1)}{4(2m-1)}\sinh\alpha(\kappa_m\cosh\alpha-\sinh\alpha)+\tfrac{1}{4}m(m-1)\cosh\alpha(\cosh\alpha-\kappa_m\sinh\alpha)\right)\tilde{c}_{m-1}$$
$$+\frac{m(m+1)(2m+1)}{4\,(2m-1)(2m+3)}\,\tilde{c}_m$$
$$-\left(\frac{(m+1)(m+2)}{4\,(2m+3)}\sinh\alpha\,(\kappa_m\cosh\alpha+\sinh\alpha)+\tfrac{1}{4}(m+1)(m+2)\right.$$
$$\left.\cosh\alpha(\cosh\alpha+\kappa_m\sinh\alpha)\right)\tilde{c}_{m+1}$$
$$+\frac{(m+1)(m+2)(m+3)}{4\,(2m+3)}\,(\cosh 2\alpha+\kappa_m\sinh 2\alpha)\;\tilde{c}_{m+2}$$
$$-\frac{m(m-1)}{2\,(2m-1)}\,(\cosh 2\alpha-\kappa_m\sinh 2\alpha)\;\tilde{e}_{m-2}$$
$$+\left(\frac{m}{2\,(2m-1)}\sinh\alpha\,(\kappa_m\cosh\alpha-\sinh\alpha)+m\cosh\alpha\,(\cosh\alpha-\kappa_m\sinh\alpha)\right)\tilde{e}_{m-1}$$
$$-\left(\frac{4\,m^3+6\,m^2-1}{2\,(2m-1)(2m+3)}+\tfrac{1}{2}(2m+1)\cosh^2\alpha+\tfrac{1}{2}\kappa_m\sinh\alpha\cosh\alpha\right)\tilde{e}_m$$
$$+\left(\frac{m+1}{2\,(2m+3)}\sinh\alpha\,(\kappa_m\cosh\alpha+\sinh\alpha)+(m+1)\cosh\alpha\,(\cosh\alpha+\kappa_m\sinh\alpha)\right)\tilde{e}_{m+1}$$
$$-\frac{(m+1)(m+2)}{2\,(2m+3)}\,(\cosh 2\alpha+\kappa_m\sinh 2\alpha)\;\tilde{e}_{m+2}$$
$$-\frac{m(m-1)(m-2)}{4\,(2m-1)}\,(\kappa_m\cosh 2\alpha-\sinh 2\alpha)\,\tilde{d}_{m-2}$$
$$+\left(\frac{m(m-1)}{4\,(2m-1)}\sinh\alpha(\cosh\alpha-\kappa_m\sinh\alpha)+\tfrac{1}{4}m(m-1)\cosh\alpha(\kappa_m\cosh\alpha-\sinh\alpha)\right)\tilde{d}_{m-1}$$
$$+\frac{m(m+1)(2m+1)}{4\,(2m-1)(2m+3)}\kappa_m\,\tilde{d}_m$$
$$-\left(\frac{(m+1)(m+2)}{4\,(2m+3)}\sinh\alpha\,(\cosh\alpha+\kappa_m\sinh\alpha)\right.$$
$$\left.+\tfrac{1}{4}(m+1)(m+2)\cosh\alpha\,(\kappa_m\cosh\alpha+\sinh\alpha)\right)\tilde{d}_{m+1}$$
$$+\frac{(m+1)(m+2)(m+3)}{4\,(2m+3)}\,(\kappa_m\cosh 2\alpha+\sinh 2\alpha)\;\tilde{d}_{m+2}$$
$$-\frac{m(m-1)}{2\,(2m-1)}\,(\kappa_m\cosh 2\alpha-\sinh 2\alpha)\;\tilde{f}_{m-2}$$
$$+\left(\frac{m}{2\,(2m-1)}\sinh\alpha\,(\cosh\alpha-\kappa_m\sinh\alpha)+m\cosh\alpha\,(\kappa_m\cosh\alpha-\sinh\alpha)\right)\tilde{f}_{m-1}$$
$$-\left(\frac{4\,m^3+6\,m^2-1}{2\,(2m-1)(2m+3)}\,\kappa_m+\tfrac{1}{2}(2m+1)\kappa_m\cosh^2\alpha+\tfrac{1}{2}\sinh\alpha\cosh\alpha\right)\tilde{f}_m$$
$$+\left(\frac{m+1}{2\,(2m+3)}\sinh\alpha\,(\cosh\alpha+\kappa_m\sinh\alpha)+(m+1)\cosh\alpha\,(\kappa_m\cosh\alpha+\sinh\alpha)\right)\tilde{f}_{m+1}$$
$$-\frac{(m+1)(m+2)}{2\,(2m+3)}\,(\kappa_m\cosh 2\alpha+\sinh 2\alpha)\;\tilde{f}_{m+2},$$

$$\chi_m = \frac{m-2}{4(2m-1)}(\cosh 2\alpha - \kappa_m \sinh 2\alpha)\,\tilde{c}_{m-2}$$
$$-\frac{1}{4(2m-1)}(m + (m-1)(\cosh 2\alpha - \kappa_m \sinh 2\alpha))\,\tilde{c}_{m-1}$$
$$+\frac{3(2m+1)}{4(2m-1)(2m+3)}\,\tilde{c}_m + \frac{1}{4(2m+3)}((m+1) + (m+2)(\cosh 2\alpha + \kappa_m \sinh 2\alpha))\,\tilde{c}_{m+1}$$
$$-\frac{m+3}{4(2m+3)}(\cosh 2\alpha + \kappa_m \sinh 2\alpha)\tilde{c}_{m+2} - \frac{(m-2)(m-3)}{2(2m-1)}(\cosh 2\alpha - \kappa_m \sinh 2\alpha)\,\tilde{g}_{m-2}$$
$$+\frac{m-2}{4(2m-1)}((4m-3)(\cosh 2\alpha - \kappa_m \sinh 2\alpha) - (4m-1))\,\tilde{g}_{m-1}$$
$$-\left(\frac{16m^3 + 24m^2 - 34m - 21}{4(2m-1)(2m+3)} + \tfrac{1}{4}(2m+1)\cosh 2\alpha + \tfrac{1}{4}\kappa_m \sinh 2\alpha \cosh\alpha\right)\tilde{g}_m$$
$$+\left(\frac{m+3}{4(2m+3)}(4m+7)(\cosh 2\alpha + \kappa_m \sinh 2\alpha) + (4m+5)\right)\tilde{g}_{m+1}$$
$$-\frac{(m+3)(m+4)}{2(2m+3)}(\cosh 2\alpha + \kappa_m \sinh 2\alpha)\tilde{g}_{m+2} + \frac{m-2}{4(2m-1)}(\kappa_m \cosh 2\alpha - \sinh 2\alpha)\,\tilde{d}_{m-2}$$
$$-\frac{1}{4(2m-1)}(\kappa_m m + (m-1)(\kappa_m \cosh 2\alpha - \sinh 2\alpha))\,\tilde{d}_{m-1} + \frac{3(2m+1)}{4(2m-1)(2m+3)}\kappa_m\,\tilde{d}_m$$
$$+\frac{1}{4(2m+3)}(\kappa_m(m+1) + (m+2)(\kappa_m \cosh 2\alpha + \sinh 2\alpha))\,\tilde{d}_{m+1}$$
$$-\frac{m+3}{4(2m+3)}(\kappa_m \cosh 2\alpha + \sinh 2\alpha)\,\tilde{d}_{m+2}$$
$$-\frac{(m-2)(m-3)}{2(2m-1)}(\kappa_m \cosh 2\alpha - \sinh 2\alpha)\,\tilde{h}_{m-2}$$
$$+\frac{m-2}{4(2m-1)}(\kappa_m(4m-1) + (4m-3)(\kappa_m \cosh 2\alpha - \sinh 2\alpha))\,\tilde{h}_{m-1}$$
$$-\left(\frac{16m^3 + 24m^2 - 34m - 21}{4(2m-1)(2m+3)}\kappa_m + \tfrac{1}{4}(2m+1)\kappa_m \cosh 2\alpha + \tfrac{1}{4}\sinh 2\alpha\right)\tilde{h}_m$$
$$+\frac{m+3}{4(2m+3)}((4m+7)(\kappa_m \cosh 2\alpha + \sinh 2\alpha) + \kappa_m(4m+5))\,\tilde{h}_{m+1}$$
$$-\frac{(m+3)(m+4)}{2(2m+3)}(\kappa_m \cosh 2\alpha + \sinh 2\alpha)\,\tilde{h}_{m+2},$$

where $\kappa_m = \coth\left(m + \frac{1}{2}\right)\alpha$.

REFERENCES

Baskurt, O. K. & Meiselman, H. J. 2003 Blood rheology and hemodynamics. *Seminars in Thrombosis and Hemostasis* **29**, 435–450.

Brenner, H. 1964 The Stokes resistance to an arbitrary particle – IV Arbitrary fields of flow. *Chem. Engng. Sci.* **19**, 703.

Brinkman, H. C. 1947 A calculation of the viscous force exerted by a flowing fluid on a dense swarm of particles. *Appl. Sci. Res.* A **1**, 27–34.

Damiano, E. R., Duling, B. R., Ley, K. & Skalak, T. C. 1996 Axisymmetric pressure-driven flow of rigid pellets through a cylindrical tube lined with a deformable porous wall layer. *J. Fluid Mech.* **314**, 163–189.

Damiano, E. R., Long, D. S., El-Khatib, F. H. & Stace, T. M. 2004*a* On the motion of a sphere in a Stokes flow parallel to a Brinkman medium. *J. Fluid Mech.* **500**, 75–101.

Damiano, E. R., Long, D. S. & Smith, M. L. 2004*b* Estimation of viscosity profiles using velocimetry data from parallel flows of linearly viscous fluids: Application to microvascular hemodynamics. *J. Fluid Mech.* **512**, 1–19.

Damiano, E. R. & Stace, T. M. 2002 A mechano-electrochemical model of radial deformation of the capillary glycocalyx. *Biophys. J.* **82**, 1153–1175.

Damiano, E. R. & Stace, T. M. 2005 Flow and deformation of the capillary glycocalyx in the wake of a leukocyte. *Phys. Fluids* **17**, 031509-1–031509-17.

Davis, A. M. J. 2001 Axisymmetric flow due to a porous sphere sedimenting towards a solid sphere or a solid wall: Application to scavenging of small particles. *Phys. Fluids* **13**, 3126–3133.

Dean, W. R. & O'Neill, M. E. 1963 A slow motion of viscous liquid caused by the rotation of a solid sphere. *Mathematika* **10**, 13–24.

Debye, P. & Bueche, A. M. 1948 Intrinsic viscosity, diffusion, and sedimentation rate of polymers in solution. *J. Chem. Phys.* **16**, 573–579.

Edwards, D. A., Hanes, J., Caponetti, G., Hrkach, J., Ben-Jebria, A., Eskew, M. L., Mintzes, J., Deaver, D., Lotan, N. & Langer, R. 1997 Large porous particles for pulmonary drug delivery. *Science* **276**, 1868–1871.

Feng, J., Ganatos, P. & Weinbaum, S. 1998 Motion of a sphere near planar confining boundaries in a Brinkman medium. *J. Fluid Mech.* **375**, 265–296.

Feng, J. & Weinbaum, S. 2000 Lubrication theory in highly compressible porous media: the mechanics of skiing, from red cells to humans. *J. Fluid Mech.* **422**, 281–317.

Ganatos, P., Pfeffer, R. & Weinbaum, S. 1980 A strong interaction theory for the creeping motion of a sphere between plane parallel boundaries. Part 2. Parallel motion. *J. Fluid Mech.* **99**, 755–783.

Goldman, A. J. 1966 Investigations in low Reynolds number fluid–particle dynamics. PhD Thesis, New York University.

Goldman, A. J., Cox, R. G. & Brenner, H. 1967 Slow viscous motion of a sphere parallel to a plane wall—II Couette flow. *Chem. Engng. Sci.* **22**, 653–660.

Goren, S. L. & O'Neill, M. E. 1971 On the hydrodynamic resistance to a particle of a dilute suspension when in the neighbourhood of a large obstacle. *Chem. Engng. Sci.* **26**, 325–338.

Halvorsen, K. 2007 Probing weak single-molecule interactions: Development and demonstration of a new instrument. PhD Thesis, Boston University.

Heinrich, V., Wong, W. P., Halvorsen, K. & Evans, E. 2008 Imaging biomolecular interactions by fast 3D-tracking of laser-confined carrier particles. *Langmuir* **24**, 1194–1203.

Hou, J. S., Holmes, M. H., Lai, W.M. & Mow, V. C. 1989 Boundary conditions at the cartilage synovial fluid interface for joint lubrication and theoretical verifications. *J. Biomech. Engng.* **111**, 78–87.

Jeffery, G. B. 1915 On the steady rotation of a solid of revolution in a viscous fluid. *Proc. Lond. Math. Soc.* **2**, 327–338.

Kargol, A., Przestalski, M. & Kargol, M. 2005 A study of porous structure of cellular membranes in human erythrocytes. *Cryobiology.* **50**, 332–337.

Kim, A.S. & Stolzenbach, K.D. 2004 Aggregate formation and collision efficiency in differential settling. *J. Colloid Interface Sci.* **271**, 110–119.

Long, D. S., Smith, M. L., Pries, A. R., Ley, K. & Damiano, E. R. 2004 Microviscometry reveals reduced blood viscosity and altered shear rate and shear stress profiles in microvessels after hemodilution. *Proc. Natl Acad. Sci. USA* **101**, 10060–10065.

Moon, P. & Spencer, D. 1961 *Field Theory Handbook*. Springer.

Nir, A. & Pismen, L.M. 1977 Simulations of interparticle forced convection, diffusion and reaction in porous catalyst. *Chem. Engng. Sci.* **32**, 35–41.

O'Neill, M. E. 1964 A slow motion of viscous liquid caused by a slowly moving solid sphere. *Mathematika* **11**, 67–74.

O'Neill, M. E. 1968 A sphere in contact with a plane wall in a slow linear shear ow. *Chem. Engng. Sci.* **23**, 1293–1298.

O'Neill, M. E. & Stewartson, K. 1967 On the slow motion of a sphere parallel to a nearby plane wall. *J. Fluid Mech.* **27**, 705–724.

Pruppacher, H. R. & Klett, J. D. 1978 *Microphysics of Clouds and Precipitation*. D. Reidel.

Saffman, P. G. 1971 On the boundary condition at the surface of a porous medium. *Stud. Appl. Maths* **1**, 93–101.

Saffman, P. G. & Turner, J. S. 1956 On the collision of drops in turbulent clouds. *J. Fluid Mech.* **1**, 16–30.

Smith, M. L., Long, D. S., Damiano, E. R. & Ley, K. 2003 Near-wall μ-PIV reveals a hydrodynamically relevant relevant endothelial surface layer in venules *in vivo*. *Biophys. J.* **85**, 637–645.

Stimson, M. & Jeffery, G. B. 1926 The motion of two spheres in a viscous fluid. *Proc. R. Soc. Lond.* **3**, 110–116.

Truesdell, C. & Toupin, R. 1960 The classical field theories. In *Handbuch der Physik* (ed. S. Flügge), pp. 226–793. Springer.

Tsapis, N., Bennett, D., Jackson, B., Weitz, D. A. & Edwards, D. A. 2002 Trojan particles: Large porous carriers of nanoparticles for drug delivery. *Proc. Natl Acad. Sci. USA* **99**, 12001–12005.

Vainshtein, P. & Shapiro, M. 2006 Porous agglomerates in the general linear flow field. *J. Colloid Interface Sci.* **298**, 183–191.

Vainshtein, P., Shapiro, M. & Gutfinger, C. 2004 Mobility of permeable aggregates: effects of shape and porosity. *J. Aerosol Sci.* **35**, 383–404.

Vink, H. & Duling, B. R. 1996 Identification of distinct luminal domains for macromolecules, erythrocytes, and leukocytes within mammalian capillaries. *Circ. Res.* **79**, 581–589.

Weinbaum, S., Ganatos, P. & Yan, Z. 1990 Numerical multipole and boundary integral equation techniques in Stokes flow. *Annu. Rev. Fluid Mech.* **22**, 275–316.

Weinbaum, S., Zhang, X., Han, Y., Vink, H. & Cowin, S. C. 2003 Mechanotransduction and flow across the endothelial glycocalyx. *Proc. Natl Acad. Sci. USA* **100**, 7988–7995.

Wong, W. P. 2006 Exploring single-molecule interactions through 3D optical trapping and tracking: From thermal noise to protein refolding. PhD Thesis, Harvard University, Cambridge, MA.

Wong, W. P. & Halvorsen, K. 2006 The effect of integration time on fluctuation measurements: Calibrating an optical trap in the presence of motion blur. *Opt. Express* **14**, 12517–12531.

Wong, W. P., Heinrich, V. & Evans, E. 2004 Exploring reaction pathways of single-molecule interactions through the manipulation and tracking of a potential-confined microsphere in three dimensions. *Mat. Res. Soc. Symp. Proc.* **790**, P5.1.1–P5.1.12.

Zhao, M. L., Chien, S. & Weinbaum, S. 2001 Dynamic contact forces on leukocyte microvilli and their penetration of the endothelial glycocalyx. *Biophys. J.* **80**, 1124–1140.